

Stable Geometry, Reversing Poles: The Bipolar Structure of AI Occupational Substitutability and Its Decade-Scale Inversion

Shuyao Gao* Minghao Huang†

June 9, 2026

Abstract

Empirical research on the labor-market impact of artificial intelligence has converged, since [Frey and Osborne \(2017\)](#), on a continuous-gradient representation in which each occupation is assigned a real-valued exposure score on $[0, 1]$ obtained by linear aggregation across capability dimensions. This continuity is rarely articulated as an assumption and has not been tested at the micro-action level where substitution actually occurs. We decompose 1,961 O*NET Detailed Work Activities into 15,817 micro-actions using a multi-agent LLM pipeline with 31-expert HITL calibration, then project the DWA-level Occupational Automation Index from our prior work onto a 7-macro semantic typology. The result is a **bipolar structure**. Tool-Mediated Physical (M2, mean OAI = 0.054) and Planning & Design (M7, mean OAI = 0.499) form two extremes separated by Cohen’s $d = 2.41$ ($H = 172.88$, $p = 6.21 \times 10^{-34}$). The geometry is robust under three independent stress tests: resolution ($K = 7$ to $K = 15$, polar gap widens from 0.45 to 0.57), encoder swap to BGE (LLM-class OAI lead replicates at $3.37\times$), and Eloundou’s GPT-4 task ratings (DWA-level $\rho = 0.635$). The six middle macros form a **low-contrast band** between the poles (TOST at $d = 0.2$ admits only 1/15 pairs as equivalent), not a flat plain. The geometry’s stability does not, however, extend to its content. Across a decade, the polarity has inverted. Frey-Osborne (2013) placed Tool-Mediated Physical near the highest computerisation risk and Planning & Design near the lowest; our LLM-era OAI reverses that order, with macro-level FO \leftrightarrow Eloundou Spearman $\rho = -0.750$, $p = 0.020$, against the original Oxford Martin appendix. Which pole is high is therefore contingent on the era’s dominant capability frontier, while the **stable geometry** itself is the structurally robust object.

Keywords: AI substitution; occupational tasks; action-level analysis; hierarchical clustering; sentence embeddings; O*NET; bipolar structure; polarity inversion; stable geometry; computational social science.

*Doctoral Student, aSSIST University, Seoul, South Korea. Email: gaoshuyao.mk@gmail.com. Code and data: <https://github.com/ShuyaoGao/bipolar-action-substrate>.

†Professor, aSSIST University, Seoul, South Korea. Corresponding author. Email: mhuang@assist.ac.kr.

1 Introduction

Research on the labor-market impact of artificial intelligence has converged, since [Frey and Osborne \(2017\)](#), on a recurring methodological architecture. An aggregate substitutability score is computed as a linear or near-linear combination of capability dimensions, and then assigned to each occupation as a real number on $[0, 1]$. [Frey and Osborne \(2017\)](#) hand-coded nine bottleneck dimensions and regressed an expert-labelled probability against them, producing a single computerisation risk for each of 702 occupations. [Felten et al. \(2021\)](#) constructed the Artificial Intelligence Occupational Exposure (AIOE) score by linearly aggregating 52 ability ratings from O*NET against 10 emergent AI applications drawn from the EFF database. [Eloundou et al. \(2024\)](#) prompted GPT-4 as a rater on every O*NET task and combined the resulting exposure variables, E_1 for the LLM-direct measure and E_2 for the LLM-plus-tools measure, into a continuous occupation-level metric. The successor literature, including ILO cross-country extensions ([Gmyrek et al., 2023](#)) and recent agentic-AI exposure work ([Gupta and Kumar, 2026](#)), has retained this aggregation pattern: rate a set of capability dimensions, take a weighted average, project onto an occupation-level scalar. The implicit assumption shared across these otherwise different studies is that substitutability lives on a continuum, with occupations smoothly distributed along a real-valued exposure axis and the central interpretive task being to locate each occupation on that axis. The continuous-gradient assumption is rarely articulated as an assumption, and to our knowledge has never been empirically tested against the actual distributional shape of the data. The consequence is non-trivial. If the underlying substitutability distribution is in fact discrete or polarised rather than continuous, occupations situated near the same aggregate score may face categorically different displacement regimes, and policy interpretations that read off “moderately exposed” or “highly exposed” from a continuous index can misclassify the structural position of every occupation in the middle of the scale.

Substitution does not happen at the occupational aggregate; it happens action by action. A radiologist’s “read a chest x-ray” may be highly substitutable while “communicate findings to the surgical team” is not, even though both contribute to the same Detailed Work Activity (DWA) and the same occupation. Recent within-occupation work has begun to document this heterogeneity using survey-based skill data ([Henseke et al., 2025](#)), but it stops at the task level. The task-based theoretical framework laid out by [Acemoglu and Restrepo \(2022\)](#) likewise treats tasks as the smallest unit of analysis. In our prior work ([Gao et al., 2026](#)), we showed that a Bottleneck (Leontief-style) aggregation of Tech and Risk factors produces a sharply non-linear DWA-level Automation Index, with values concentrated on a discrete subset $\{0, 0.3, 0.5, 0.7, 1.0\}$ rather than smoothly filling the $[0, 1]$ interval. The non-linearity was a clue that something other than a continuous gradient was operating beneath the aggregate, but the source of the non-linearity remained underspecified at the DWA level. The natural next question, and the one we address here, is whether the underlying micro-action structure itself is continuous, or whether the gradient is an aggregation artifact masking a discrete substrate. Answering this requires decomposing each DWA into its constituent micro-actions and asking what shape the substitutability distribution takes when nothing is aggregated away.

A second strand of contemporary discussion runs parallel to the gradient tradition. Capability-stage frameworks now dominate industry roadmaps. [Morris et al. \(2024\)](#) propose six AGI levels

for tracking model performance breadth and depth, and OpenAI’s internal five-stage progression (Chatbots, Reasoners, Agents, Innovators, Organizations) was disclosed in Metz (2024). A series of consulting forecasts have read off occupation-by-occupation displacement projections from these stages. Chui et al. (2023) estimate \$2.6–4.4 trillion in annual added value from generative AI across 63 use cases, and Ellingrud et al. (2023) project that up to thirty percent of U.S. work hours could be automated by 2030, with twelve million occupational transitions concentrated on lower-wage workers. These forecasts share a structural property: each takes a contemporaneous snapshot of model capabilities, applies it forward, and projects exposure as a function of the projected capability trajectory. They are point predictions about content, not predictions about structure. What we show in this paper is that the structure, the geometry of which actions cluster together at which substitutability level, has remained remarkably stable across a decade, while the content, which cluster sits at the high-exposure pole and which sits at the low, has inverted entirely.

We decompose 1,961 DWAs into 15,817 micro-actions using a multi-agent LLM pipeline calibrated against the 31-expert human-in-the-loop panel reported in Gao et al. (2026). Sentence-BERT embeddings of every micro-action description are reduced via UMAP, clustered first by HDBSCAN into 35 micro-clusters, and then aggregated by hierarchical Ward linkage into seven macro-clusters. These seven macros differentiate along three independent dimensions: process stage (Intent, Navigation, Perception, Manipulation, Feedback), cognitive-physical orientation, and sequential position within the DWA workflow. Projecting the DWA-level Automation Index from Gao et al. (2026) onto this typology yields a **bipolar structure**. Two extreme macros, Tool-Mediated Physical Execution (M2, mean OAI = 0.054) and Planning & Design (M7, mean OAI = 0.499), are separated by a Cohen’s d of 2.41 (Mann-Whitney $p < 10^{-33}$ after Bonferroni correction). The geometry is robust to clustering resolution (the polar gap widens from 0.45 at $K = 7$ to 0.57 at $K = 12$ and $K = 15$), to encoder family (the LLM-class OAI lead replicates under BGE labelling at $3.37\times$), and to indicator choice (Eloundou’s GPT-4 task ratings reproduce the bipolar pattern with Cliff’s $\delta = 0.902$ for the M2 versus M7 extreme pair). The six middle macros do not collapse the contrast; they occupy a low-contrast band in which two-one-sided tests at $d = 0.2$ admit only 1 of 15 pairs as equivalent. Against this spatial stability sits a temporal reversal. The same macros under Frey-Osborne’s 2013 computerisation probability take a polar ordering that is the exact inverse of their LLM-era OAI ordering, with macro-level Spearman $\rho = -0.750$, a result we label **polarity inversion**. The geometry is stable; the polarity is not.

We make four contributions:

1. **Methodologically**, we present a multi-layer clustering pipeline applied to occupational micro-actions with a reproducible validation cascade combining Hartigan dip testing, Kolmogorov-Smirnov goodness-of-fit testing, Bonferroni-corrected pairwise non-parametric tests, two-one-sided equivalence tests, and a resolution sweep across $K = 7$ –15.
2. **Empirically (spatial axis)**, we provide direct evidence that occupational AI-substitutability is bipolar with a low-contrast middle, and that this geometry is robust under three independent stress tests: clustering resolution (the gap widens, not narrows, as K grows), encoder family (MPNet and BGE both reproduce the LLM-class OAI lead within $0.2\times$),

and indicator choice (Eloundou’s GPT-4 task exposure independently reproduces the M2 versus M7 polarity with $\delta = 0.902$).

3. **Empirically (temporal axis)**, we document a decade-scale polarity inversion: the same macros under Frey-Osborne’s 2013 probability and our LLM-era OAI take opposite polar orderings (macro-level Spearman $\rho = -0.750$, $p = 0.020$, computed against the original Oxford Martin appendix data). The shape persists; the polarity reverses.
4. **Theoretically**, we offer a mechanistic reading of the polarity through a four-way intelligence-type classification (Linguistic / Multimodal Perception / Embodied / Human-Bound) that independently predicts OAI ($H = 527.6$, LLM-class mean OAI 0.427 versus other classes’ mean 0.127): the era’s dominant AI capability determines which intelligence type maps to the high-exposure pole, and so a single-point exposure forecast inherits the era’s capability frontier and reverses with it.

Section 2 reviews the gradient tradition, the action-level decomposition literature, embedding-based occupational analysis, and the capability-stage and wave-forecast frameworks we critically position. Section 3 details data, pipeline, embedding, clustering, intelligence-type labelling, and external-indicator alignment. Section 4 presents the spatial axis: typology, multi-dimensional differentiation, bipolar OAI distribution, the M4 chimera as a self-applied resolution-aggregation critique, M2 internal bifurcation, the generic substrate, external-indicator reproduction, and intelligence-type prediction of OAI. Section 5 presents the temporal axis: era gradient, polarity inversion, and synthesis. Section 6 discusses implications for substitution theory, the RPA-AI boundary, the generic substrate, the present wave of forecasts, methodology, and limitations. Section 7 concludes.

2 Related Work

2.1 The Continuous-Gradient Tradition

The first generation of empirical AI-substitutability studies established the methodological architecture we problematize in this paper. [Frey and Osborne \(2017\)](#) hand-coded each of 702 U.S. occupations against nine bottleneck dimensions drawn from the engineering literature on what robots and pattern-recognition algorithms cannot yet do, then regressed an expert-labelled binary classification ($n = 70$) to project a continuous computerisation risk onto the remaining occupations. The output is a single $[0, 1]$ -valued score per occupation, exactly the gradient form we identify as the field’s default. [Felten et al. \(2021\)](#) introduced the Artificial Intelligence Occupational Exposure (AIOE) dataset, mapping 52 ability ratings from O*NET against 10 emergent AI applications via Mechanical Turk crowd ratings; the resulting score is a linear sum of ability-weighted application exposures, again projected as a continuous occupation-level scalar. [Webb \(2020\)](#) approached the same problem from the technology side, matching verb-noun pairs in occupational task descriptions against the verb-noun structures of AI-related patent abstracts to compute a continuous patent-exposure index. [Eloundou et al. \(2024\)](#) replaced human raters with GPT-4 and prompted the model directly for exposure ratings on each O*NET task, combining the resulting variables E_1 (LLM-direct) and E_2 (LLM-plus-tools) into a continuous

occupation-level metric and concluding that approximately 80% of U.S. workers have at least 10% of their tasks exposed at E_1 . [Gmyrek et al. \(2023\)](#) extended the GPT-rating approach to a cross-country setting, combining task-exposure scores with national occupational mixes to estimate aggregate AI exposure across more than 60 countries. The default downstream interpretive frame, in which one reads off what fraction of the workforce is “highly,” “moderately,” or “minimally” exposed, inherits the continuity premise: cut points on a continuous distribution are stipulated rather than estimated. Even where rich auxiliary data is brought in, such as occupation-level wages, employment shares, or regional concentration, the auxiliary structure decorates rather than disrupts the underlying scalar. The continuous index is the dependent variable, and the empirical machinery is built to predict it. Methodological refinements within this tradition, including the move from human raters to crowd raters to LLM raters and the move from US-only to cross-country settings, preserve the linear-aggregation step that produces the scalar. The structural commonality is unambiguous: each study reduces a multi-dimensional capability profile to a continuous occupation-level scalar and treats that scalar as the empirical object of analysis. None of them examines whether the underlying substitutability distribution is in fact continuous, polarised, or mixture-shaped before fitting summary statistics to it. The empirical question of distributional shape, the question we take up in this paper, is structurally outside the frame these studies occupy.

2.2 Action-Level Decomposition

A separate strand of the literature works at finer occupational granularities. [Acemoglu and Restrepo \(2018\)](#) formalize the task-based theoretical framework in which automation displaces specific tasks rather than entire occupations, decomposing aggregate labor demand into the contribution of automated and non-automated tasks. [Acemoglu and Restrepo \(2022\)](#) link this framework to U.S. wage inequality through a quantitative model in which task displacement explains a substantial share of the post-1980 college-noncollege wage gap. In both cases, however, “tasks” remain a theoretical abstraction. The empirical implementation aggregates O*NET task data and uses occupation-level moments rather than decomposing tasks further. [Henseke et al. \(2025\)](#) introduce within-occupation heterogeneity as an empirical phenomenon, using UK Skills and Employment Survey data to show that AI exposure varies substantially across workers within the same nominal occupation; this is an important precursor to action-level analysis, but it stops at the task level and does not cluster the underlying actions into a typology. The recent Agentic Task Exposure framework ([Gupta and Kumar, 2026](#)) extends task exposure to multi-step agentic AI capabilities (planning, tool use, multi-step reasoning) but inherits the linear-gradient aggregation of the AIOE and Eloundou tradition. In our own prior work, [Gao et al. \(2026\)](#) disaggregated occupations into 2,087 DWAs and applied a Bottleneck (Leontief-style) aggregation of separate Tech and Risk factors. The Bottleneck operator $\min(\cdot)$ enforces the intuition that a single non-automatable step in a workflow blocks the entire workflow from being automated, regardless of how cheaply other steps can be replaced. The resulting DWA-level Automation Index is concentrated on the discrete set $\{0, 0.3, 0.5, 0.7, 1.0\}$, showing that even at the DWA level the substitutability distribution departs from continuity. That work also identified *Cognitive Risk Asymmetry*, a systematic +0.35 inflation in expert-perceived risk relative

to AI-rated risk in high-stakes regulatory domains, as a structural feature operating beneath the aggregate. What that paper did not specify, and what the present paper supplies, is the underlying micro-action structure that produces these aggregate-level non-linearities. The closing observation is structural: no published study has clustered occupational micro-actions, applied unsupervised dimensionality reduction to occupational text at the action level, or empirically tested whether the resulting substitutability distribution is continuous, multi-modal, or polarised.

2.3 Embedding-Based Occupational Analysis

A third strand of the literature uses computational text representations of occupational data, primarily for occupation mobility and skill-content analysis, without engaging directly with substitutability. [Autor et al. \(2003\)](#) initiated the routine-versus-non-routine task measurement framework that grounds Routine-Biased Technological Change (RBTC). Their O*NET-derived task indices, computed by hand-coding the routine versus non-routine and cognitive versus manual content of occupational descriptions, remain a foundational reference point. [Deming and Noray \(2020\)](#) introduce task-vector cosine similarity computed over O*NET task descriptions to model occupational mobility, treating each occupation as a high-dimensional point and measuring transition probability via embedding distance. This is an early instance of vector representations used for occupational analysis. Recent applications of sentence-BERT ([Reimers and Gurevych, 2019](#)) and MPNet ([Song et al., 2020](#)) to human-resources and labor-market problems, including automated job classification, resume-to-job matching, and occupational skill-graph construction, show that off-the-shelf semantic encoders capture occupational structure adequately for downstream analytic tasks, even without domain-specific fine-tuning. The methodological apparatus we deploy, UMAP ([McInnes et al., 2018](#)) for dimensionality reduction and HDBSCAN ([Campello et al., 2013](#)) for density-based clustering, comes from the same toolkit that has been used elsewhere for biomedical text, scientific document organization, and consumer-review topic discovery, but to our knowledge has not been applied at the resolution of occupational micro-actions. The pipeline we present in this paper synthesizes all three strands: we apply sentence-embedding methods (third strand) to action-level occupational data (second strand) and use the resulting typology to test a distributional question raised by the first strand. The synthesis is what makes the test possible. Without action-level decomposition there is no granular substrate; without sentence embeddings there is no scalable way to compare 15,817 actions; and without distributional testing the resulting clusters would be merely descriptive. No prior study has clustered occupational micro-actions or empirically tested whether the substitutability distribution they imply is continuous. The present paper does both.

2.4 Capability-Stage Frameworks and Wave Forecasts

A fourth strand sits alongside the academic literature. It comprises capability-stage frameworks issued by research labs and consulting firms, together with the wave-of-displacement forecasts that read off occupation-level projections from those frameworks. These frameworks position the temporal axis of substitutability that the present paper takes up empirically, so we summarise them here as the conceptual context for our temporal results (§5). Two academic-adjacent capability-level proposals organise the contemporary discussion. [Morris et al. \(2024\)](#) propose a

six-level taxonomy of AGI performance breadth and depth (No AI, Emerging, Competent, Expert, Virtuoso, Superhuman) with explicit principles for distinguishing system-level capability from task-level capability and for tying advances on each axis to deployment considerations. OpenAI’s internal five-stage progression of Chatbots, Reasoners, Agents, Innovators, and Organizations was disclosed publicly through Metz (2024) as part of internal safety communication; we treat the Bloomberg account as the canonical source and note that it is an industry framework rather than a peer-reviewed proposal. Both frameworks operationalise the intuition that AI capability advances unfold in discrete stages, with each stage unlocking a distinct class of occupational substitutability.

Consulting forecasts have used these capability-stage scaffolds to read off occupation-by-occupation displacement projections. Chui et al. (2023) estimate that generative AI could add an annual \$2.6–4.4 trillion to the global economy across 63 use cases, with potential productivity boosts ranging from 0.5% to 3.4% depending on the pace of adoption. Ellingrud et al. (2023) project that up to 30% of current U.S. work hours could be automated by 2030, with twelve million occupational transitions concentrated disproportionately on lower-wage workers. These forecasts share a structural property worth emphasising. Each takes a contemporaneous snapshot of AI capabilities and projects a wave of displacement forward in time as a function of capability trajectory. They are predictions about which occupations sit at which exposure level under tomorrow’s capabilities, not predictions about whether the structural geometry of the exposure distribution will persist. This is precisely the gap our temporal analysis addresses. By comparing the polar ordering produced by 2013-era capability-bottleneck reasoning (Frey and Osborne, 2017) against the polar ordering produced by 2023-era LLM-rating capability (Eloundou et al., 2024), we ask whether the structural ordering itself is stable across capability eras. A negative answer, which we find, implies that any single-point projection inherits the era’s capability frontier and inverts when the frontier moves. A more thorough comparison of action-level micro-structure against the wave-forecast level is a natural next step beyond the scope of the present paper, and we develop it in separate work currently in preparation.

2.5 Microfoundations and Routine Dynamics

The four strands above locate the present paper within the AI-exposure literature. A fifth strand, drawn from organisation theory rather than from computational labour economics, supplies the theoretical commitment that motivates our analytical unit. The *microfoundations* programme (Coleman, 1990; Felin and Foss, 2005; Felin et al., 2012, 2015) holds that organisation-level phenomena, including firm capability, strategic heterogeneity, and technological adaptation, must in principle be explainable in terms of the individual-level actions, interactions, and cognitions that compose them. The methodological corollary is sharp: aggregate analyses that stop at coarser units of observation are ontologically incomplete with respect to the mechanisms they invoke. *Routine dynamics* (Pentland and Feldman, 2005; Feldman and Pentland, 2003; Pentland et al., 2012) extends this commitment to the temporal dimension. Organisational routines are patterned action sequences with a *performative* aspect (the action as executed in a specific instance) and an *ostensive* aspect (the action as abstract structure recognisable across instances). The granularity at which one resolves either aspect is itself a substantive parameter of analysis,

not a methodological convenience.

Both traditions converge on a methodological commitment that has been more often stated than empirically operationalised: substantive analysis of organisational and labour-market change requires going below the standard analytical unit. The labour-substitutability literature has incrementally honoured this commitment, moving from occupation-level exposure scores to task-level decompositions (Acemoglu and Restrepo, 2018, 2022), and recently to within-occupation heterogeneity at the worker level (Henseke et al., 2025), but it has not yet decomposed below the task. The present paper instantiates the microfoundational commitment one layer deeper, for the AI-substitutability literature specifically. The 15,817 micro-actions are a literal implementation of action-as-analytical-unit, and the bipolar geometry we document at that resolution is therefore not just a statistical curiosity but evidence that *capability heterogeneity at the micro-action level has macro-economic consequences* that aggregate analyses cannot detect by construction. Read through this lens, the smooth-substitutability appearance documented by the gradient tradition (§2.1) is the macro-level shadow of a discrete micro-action substrate that those analyses cannot resolve. Our temporal-axis result (§5) supplies a routine-dynamics reading: which micro-action types confer competitive insulation is itself a function of the era’s dominant capability frontier, so the ostensive identity of a “substitution-resistant” routine is era-contingent even when its performative composition is stable.

3 Data and Method

3.1 Data Construction

We took as our base the O*NET 30.2 release of the U.S. occupational ontology, which catalogues 923 detailed occupations linked to 2,087 Detailed Work Activities (DWAs). DWAs are the finest grain at which O*NET labels work; below them, the ontology is silent. Closing this gap is the empirical premise of the present paper.

To decompose each DWA into a micro-action sequence, we applied a multi-agent LLM pipeline that inherits its variance-driven HITL calibration backbone from our prior work (Gao et al., 2026). For every DWA, **four locally-deployed open-weight LLMs** independently produced 5–12 step sequences against a fixed schema; each model then read the full set of drafts and produced a synthesized version; finally each model voted on the best of the four synthesized candidates. Auto-resolution at 3:1 or stronger consensus accepted the majority draft directly ($n = 1,564$ DWAs). The 502 contested cases that fell short of this threshold were arbitrated by **three frontier-class models** under the same voting scheme; 397 reached a 2-of-3 consensus and entered the dataset. The remaining 126 cases (105 cases where neither stage produced majority agreement, plus 21 cases where one of the four local models failed to return a vote) were dropped to preserve label quality. The DWA conservation identity therefore holds: $1,564 + 397 + 126 = 2,087$.

The resulting **Final Golden Dataset** comprises **1,961 DWAs decomposed into 15,817 micro-actions**. Each micro-action carries five structured fields: `step_order` (integer position 1–13 within its sequence), `action_description` (free text), `mapped_stage` (one of five canonical process stages: `Intent_Communication`, `Navigation_Addresssing`, `Perception_Diagnosis`,

Table 1: Data scale summary.

Quantity	Value
O*NET occupations	923
O*NET DWAs (baseline)	2,087
DWAs surviving multi-agent decomposition	1,961
Total micro-actions	15,817
Steps per DWA (mean / median / std)	8.07 / 8 / 1.34
mapped_stage categories (canonical)	5
cognitive_or_physical buckets (normalized)	4
Resolution: 4-local-LLM majority	1,564 (79.8%)
Resolution: 3-frontier 2-of-3 consensus	397 (20.2%)
Dropped (joint disagreement + missing votes)	126 (6.0%)
HITL backbone	inherited from Gao et al. (2026)

Manipulation_Execution, or Feedback_Verification), cognitive_or_physical (Cognitive, Physical, mixed, or other, after normalization of 39 LLM-emitted lexical variants), and key_challenge (free text). The mean DWA contains 8.07 micro-actions (median 8; standard deviation 1.34; range 5–13). Table 1 summarizes the data scale.

3.2 Embedding

We embedded every action_description into 768-dimensional vectors using the off-the-shelf sentence-transformers/all-mpnet-base-v2 model ([Reimers and Gurevych, 2019](#); [Song et al., 2020](#)). The MPNet base architecture combines masked-language and permuted-language objectives, and all-mpnet-base-v2 is a widely-adopted general-purpose sentence encoder with strong performance on standard semantic similarity benchmarks. Inputs were not truncated. We used a batch size of 64, no gradient updates, and no domain-specific fine-tuning. Choosing not to fine-tune was deliberate. Testing whether off-the-shelf semantic similarity is already adequate for occupational micro-actions is itself an empirical question. If the resulting clusters prove interpretable and externally valid (§4), the answer is yes, and further fine-tuning becomes an optimization rather than a necessity.

3.3 Dimensionality Reduction

Sentence embeddings at 768-d are too noisy for density-based clustering and too high-dimensional for interpretable visualization. We therefore reduced dimensionality with UMAP ([McInnes et al., 2018](#)) in two parallel configurations.

For visualization we projected to 2-d with `n_neighbors=30, min_dist=0.1, metric='cosine'`. For clustering we projected to 5-d with `n_neighbors=30, min_dist=0.0, metric='cosine'`. Both runs fixed `random_state=42`. The 2-d configuration optimizes for global readability of the topology (Fig. 1); the 5-d configuration preserves more local distance structure for downstream HDBSCAN.

Five dimensions for clustering is a conservative compromise. UMAP is topology-preserving but not metric-preserving ([McInnes et al., 2018](#)), so collapsing all the way to 2-d before clustering risks discarding structure that would still be locally separable in the original 768-d space. Five dimensions retains enough local variance for HDBSCAN’s mutual-reachability distance to behave

well, while keeping computation trivial. The choice of 5-d over 10-d or 20-d was empirical: at higher target dimensions the resulting micro-cluster count grew without bringing visible semantic improvement to cluster TF-IDF profiles. Both UMAP outputs were cached on disk for reproducibility, so no UMAP stochasticity contaminates the statistical tests in §3.5.

3.4 Clustering Pipeline

We employed a **two-stage hierarchical procedure** to extract structure at two distinct granularities.

Stage 1, micro-clustering with HDBSCAN. We applied HDBSCAN (Campello et al., 2013) to the 5-d UMAP space with `min_cluster_size=100`, `min_samples=20`, `cluster_selection_method='eom'`, and Euclidean distance. The minimum cluster size was set at 100 to ensure every surviving cluster contained enough samples to support downstream stratified analyses. HDBSCAN identified **35 micro-clusters** containing 10,180 micro-actions; the remaining **5,637 micro-actions (35.6%) fell into the noise label -1**. A core methodological decision was to **not** force these noise points into their nearest cluster. Section 4.6 treats this group as a structural finding rather than an algorithmic failure.

Stage 2, macro-clustering with hierarchical Ward linkage. To group the 35 micro-clusters into a smaller, interpretable typology, we built a **15-d feature vector per micro-cluster**:

- 5 dimensions: mean of the cluster’s UMAP-5d coordinates (the cluster’s centroid in semantic space);
- 5 dimensions: relative frequency of each canonical `mapped_stage`;
- 4 dimensions: relative frequency of each normalized `cognitive_or_physical` bucket;
- 1 dimension: mean `step_order`.

Each dimension was z-score normalized across the 35 micro-clusters to prevent scale dominance. Without normalization, the centroid coordinates carry variance roughly five times larger than the proportion features. We then computed Ward linkage (Murtagh and Legendre, 2014) on the resulting 35×15 matrix.

Inspecting the dendrogram for natural break points, we observed three large jumps in linkage distance: a 4.63-unit gap between $K = 2$ and $K = 3$, a 1.86-unit gap between $K = 3$ and $K = 4$, and a 1.74-unit gap between $K = 7$ and $K = 8$. $K = 2$ is too coarse to be informative; $K = 3$ yields only a coarse physical, cognitive, and meta separation. We traced the merging behaviour from $K = 4$ through $K = 6$ against the eventual $K = 7$ partition. **At** $K = 4$ the cut conflates the eventual M5, M6, and M7 micros into a single 16-member super-macro that contains every cognitive-and-coordination theme (verification, person-centred service, planning), and similarly merges the eventual M1 and M2 micros into a 9-member physical block. **At** $K = 5$ the verification-and-stakeholder-reporting group (eventual M5) splits off, but M6 and M7 remain conflated in a 12-member group and the physical block remains intact. **At** $K = 6$ the physical block finally bifurcates into the eventual M1 (locating-and-provisioning) and M2

(tool-mediated execution), yet M6 and M7 are still merged despite disjoint top-15 TF-IDF profiles (M6: *patient, client, customer*; M7: *project, specifications, design*) and cognitive-physical ratios that differ by 14 percentage points (70% vs 84% Cognitive). Only at $K = 7$ does the M6 versus M7 separation materialize. $K = 8$ and beyond produce additional singletons beyond C9 without further substantive splits at the headline level. The more aggressive $K = 12$ and $K = 15$ cuts that we report in the resolution sweep (§4.3) further bifurcate M4 along its internal cognitive-physical axis, which we analyse separately as a chimera diagnosis (§4.4). We therefore selected $K = 7$ as the headline cut.

At $K = 7$ the raw Ward output places C9 in its own one-member macro. Rather than absorb it into a neighbour to satisfy the every-macro- ≥ 2 -members heuristic, we preserved it as a distinct macro (M3) because the singleton status is the substantive finding: the micro-cluster’s “repeat steps” content is a meta-action that scaffolds other domains rather than constituting a domain of its own. This decision is justified empirically in §4.5.

The final analytical structure is therefore **7 macros (M1 to M7), 1 noise group, and 1 mixed-DWA group**. The mixed-DWA group is defined at the DWA level: a DWA whose largest macro-share is below 0.40 is reassigned from its (weak) dominant macro to a separate `mixed_dwa` cell. We chose the 0.40 threshold rather than 0.50 because micro-action sequences are constitutively spread across multiple stages by design. Most DWAs touch three to five macros in their 5 to 13 actions, so requiring a strict majority would over-classify well-typed DWAs as mixed and erode statistical power. A 0.30 threshold, by contrast, would let the largest of three roughly equal shares claim dominance. At 0.40 only 96 of 1,961 DWAs (4.9%) fall into `mixed_dwa`, while every retained dominant assignment outpolls every alternative individually. Figure 1 plots all 15,817 micro-actions in UMAP-2d, coloured by macro membership.

3.5 OAI Projection and Statistical Tests

We projected the **DWA-level Automation Index** computed by Gao et al. (2026) onto our action-level typology. In that work, this index is constructed via a Tech-Risk Dual-Factor mapping function $f(T_i, R_i)$ that integrates a four-LLM-ensemble assessment of technical capability ($T_i \in \{0, 1, 2, 3\}$) with a business-risk score ($R_i \in \{1, 2, 3, 4, 5\}$) capturing physical, legal, and compliance frictions. The mapping is piecewise: the index *AI* takes only the discrete values $\{0, 0.3, 0.5, 0.7, 1.0\}$. $R_i = 5$ (or $T_i = 0$) vetoes automation entirely ($AI = 0$); $R_i = 4$ caps automation at 0.3 for capable tasks ($T_i \in \{2, 3\}$) and at 0 otherwise; the higher tiers $\{0.5, 0.7, 1.0\}$ are reached only when both technical capability is moderate-to-high and risk is at most 3. The per-DWA scores were calibrated against a 31-expert variance-based stratified HITL panel that surfaced the +0.35 risk-score inflation Gao et al. (2026) term *Cognitive Risk Asymmetry*. The released DWA-level table (`output_10_DWA_Automation_Index.csv`) is the input to the present projection; we follow the broader literature in referring to these values as **OAI** throughout. The OAI file covers all 2,087 baseline DWAs; the 1,961 clustered DWAs match perfectly, with zero missing values.

Each DWA was assigned to its dominant macro, the macro containing the largest fraction of its micro-actions. DWAs with `dominant_share` < 0.40 were instead assigned to the `mixed_dwa` group, on the rationale stated in §3.4. M3 is structurally absent from the projection: no DWA

has M3 as its most-frequent macro, because every DWA in which C9 actions occur has them as minority steps. We treat this absence as a finding rather than a problem (§4.5) and confine OAI testing to the remaining 8 groups: M1, M2, M4, M5, M6, M7, Noise, and `mixed_dwa`.

The projection is external validation, not an input to clustering. It is worth stating explicitly what role the OAI plays in our analysis, because the role is unconventional in the AI-substitutability literature and is easy to misread. The action-level typology of §3.4 is constructed entirely from micro-action features: MPNet sentence embeddings of 15,817 individual micro-action descriptions, UMAP reduction, HDBSCAN micro-clustering, and Ward macro-clustering on a 15-dimensional feature vector composed of semantic centroid coordinates, canonical-stage shares, cognitive-physical-bucket shares, and mean sequential position. No OAI value, no DWA-level exposure score, and no occupation-level exposure score enters the pipeline at any stage. The bipolar topology of the typology, the multi-dimensional differentiation across stage, cognitive-physical orientation, and sequential position (§4.2), and the M4 chimera self-diagnosis (§4.4) are all properties of the micro-action substrate itself, independent of any substitutability scoring. The OAI projection is a separate downstream operation: we take an externally calibrated DWA-level index from Gao et al. (2026) and ask whether the bipolar topology already present in the typology aligns with the discrete-grid OAI distribution. It does, with $H = 172.88$ and a Cohen’s d of 2.41 between the two extreme macros (§4.3). The external-indicator reproduction in §4.7 then asks whether the same alignment holds under three further indicators, computed entirely outside our pipeline, namely Eloundou’s GPT-4 task labels, Felten’s AIOE, and Frey-Osborne’s computerisation probability. It does, in every case (Cliff’s $\delta = 0.902$ for the extreme pair under Eloundou, 0.79 under OAI). The clustering pipeline is therefore not circular with respect to OAI, and the bipolar finding is not an artifact of the OAI’s discrete five-point grid. The within-DWA assignment of constituent micro-actions to the dominant macro is a downstream bookkeeping step for projecting an externally calibrated DWA-level score onto an independently constructed typology, not a step in the construction of the typology itself.

We applied a primary battery of five tests and an extended robustness battery of three more.

Primary battery.

1. **Kruskal-Wallis** non-parametric ANOVA across the 8 groups, testing the global null that all groups share the same OAI distribution.
2. **Pairwise Mann-Whitney U** with Bonferroni correction across $\binom{8}{2} = 28$ pairs.
3. **Effect sizes:** Cliff’s δ (non-parametric) and Cohen’s d (parametric supplement).
4. **Hartigan dip test** (Hartigan and Hartigan, 1985) on M2’s OAI distribution to test unimodality.
5. **Two-sample Kolmogorov-Smirnov test** between the noise-group OAI and the full-population OAI.

Robustness battery (introduced in this paper).

6. **Resolution sweep across $K = 7, 8, 10, 12, 15$.** We re-cut the Ward dendrogram at five resolutions, reassign DWAs to dominant macros at each K , and recompute the Kruskal-

Wallis H , pole positions, and middle-pair non-significance rate. This tests whether the bipolar shape is an artifact of the headline $K = 7$ resolution or a structural feature of the dendrogram.

7. **Two-one-sided tests (TOST) for equivalence** on the six middle macros, at primary margin $\delta_d = 0.2 \times \sigma_{\text{pool}} = 0.060$ (Cohen’s $d = 0.2$, with σ_{pool} computed across the pooled middle six groups) and at robustness margin $\delta_{\text{abs}} = \pm 0.05$ on the absolute OAI scale. M2 versus M7 is used as a sanity check: TOST must reject equivalence on the extreme pair under any reasonable margin, else the setup is broken.
8. **External-indicator reproduction** of the bipolar pattern under three indicators not used in our pipeline: [Eloundou et al. \(2024\)](#) GPT-4 task labels (the cleanest cross-method check), [Felten et al. \(2021\)](#) AIOE ability ratings, and [Frey and Osborne \(2017\)](#) computerisation probability (the era-comparison anchor). Alignment details are given in §3.7.

All tests report both raw and corrected p -values where applicable. Effect sizes are reported on every pairwise contrast that drives a substantive claim. All random-state-sensitive procedures used `random_state=42`; library versions for full reproducibility are catalogued in `paper2_artifacts/INDEX.md`.

3.6 Intelligence-Type Labelling

For the mechanistic analysis in §4.8, we classify each micro-action into one of four intelligence types: **Linguistic** (reading, writing, computation over text), **Multimodal Perception** (visual or auditory inspection of physical state), **Embodied** (manipulation of physical objects), or **Human-Bound** (interpersonal trust, judgement, counselling, or legal accountability). The four types operationalise the AI-capability axis the era-comparison literature implicitly assumes: each type maps to a distinct technical bottleneck that contemporary AI systems either have crossed (Linguistic, increasingly Multimodal) or have not (Embodied, Human-Bound).

Status of the four-way decomposition. The four intelligence types are an *explanatory lens* for interpreting the unsupervised action-level clustering structure, not a new classification theory proposed by this paper. The contemporary literature offers multiple decompositions of AI capability that overlap with ours at different granularities. [Morris et al. \(2024\)](#) propose a six-level performance ladder crossed with a binary general-versus-narrow axis. The OECD AI Capability Indicators ([OECD, 2025](#)) use nine ability domains (Language, Social interaction, Problem solving, Creativity, Metacognition, Knowledge, Vision, Manipulation, Robotic intelligence) crossed with five capability levels. [Metz \(2024\)](#) stage capability through five sequential tiers: Chatbots, Reasoners, Agents, Innovators, and Organizations. We adopt the four-way decomposition into Linguistic, Multimodal Perception, Embodied, and Human-Bound types for three specific reasons. First, the four classes correspond to the four primary technical bottlenecks that contemporary AI systems face, which makes the lens interpretable for occupational substitutability rather than for capability tracking in general. Second, the 150-row human audit (Appendix E) validates the BGE-encoder labels against human ground truth at $\kappa = 0.893$, which is adequate for our use case but does not by itself privilege four-way over other granularities. Third, the four-way scheme sits

at a workable midpoint between Morris’s two-axis grid and OECD’s nine-by-five matrix, granular enough to separate the action-level mechanism we report in §4.8 but coarse enough to remain interpretable. **We do not claim that this four-way decomposition is uniquely correct, nor that four-way granularity is the only defensible choice.** We claim only that it is adequate for the interpretive role it plays here, which is to provide a mechanistic reading of the bipolar OAI distribution (§4.8) and its decade-scale polarity inversion (§5). Section 6.8 returns to this point as a stated limitation. Future work using finer or differently-cut intelligence-type taxonomies, including Morris-level or OECD-domain decompositions, would be a legitimate extension of the present analysis rather than a contradiction of it.

We use a prototype-anchored nearest-centroid procedure. For each class, the authors selected eight prototype actions whose intelligence-type assignment is unambiguous by construction (for instance, “draft a maintenance schedule. . .” for Linguistic, and “visually inspect equipment for signs of wear. . .” for Multimodal Perception). Each prototype was embedded into the encoder space, and the class centroid was computed as the mean of its eight prototype embeddings. Each of the 15,817 micro-actions was assigned the class of its nearest centroid (cosine similarity), with softmax confidence reported at temperature $\tau = 0.05$.

Encoder choice. For this supervised classification step we use BAAI/bge-large-en-v1.5 (Xiao et al., 2024) rather than the MPNet encoder used for clustering in §3.2. The two steps differ in what ground truth is available. Clustering is unsupervised: there is no human label for “correct cluster membership,” so an off-the-shelf general-purpose encoder is the natural choice. The four-class intelligence-type classification, in contrast, has external ground truth: the operational definitions can be applied by a human reader to any action. We constructed a 150-row stratified human-audit sample, hand-labelled the actions against the four-class operational definitions, and compared each encoder’s labels against the human ground truth: BGE labels match the human at $\kappa = 0.893$ (92.0% accuracy), MPNet labels match at $\kappa = 0.769$ (82.7%). The accuracy gap concentrates entirely on the 30 audit rows where the two encoders disagreed (BGE 70% versus MPNet 23%); on the 120 rows where the encoders agreed, both match the human at 97.5%. We therefore adopt BGE as the encoder of record for the intelligence-type analysis, with the MPNet results retained in Appendix D as a robustness check (the qualitative conclusions match). Full audit details are in Appendix E.

Theoretical grounding in the resource-based view and microfoundations. The four-way decomposition we deploy here is not an ad-hoc engineering choice; it operationalises two convergent threads in organisation theory. The *resource-based view* (Penrose, 1959; Barney, 1991; Grant, 1996) holds that firm-level capability is composed of heterogeneous, imperfectly imitable resources whose competitive value derives from the substitutability of the inputs that can perform them. Linguistic, Multimodal-Perception, Embodied, and Human-Bound capacities are precisely such resources, distinguished by the technological substitutability of the capital that can execute them: Linguistic capacity is now broadly substitutable by general-purpose language models; Embodied capacity is not yet broadly substitutable by general-purpose robotics; Human-Bound capacity is structurally non-substitutable for institutional reasons rather than technical ones. The *microfoundations programme* (Felin and Foss, 2005; Felin et al., 2012, 2015) closes the

inferential loop: macro-level organisational outcomes (a firm’s exposure to AI substitution, an occupation’s wage trajectory) must be explainable by the micro-level composition of the actions that constitute them. Reading the four classes through these two lenses fixes our analytical posture: the bipolar OAI distribution we report in §4.3 is not a description of which occupations are exposed but evidence of which capability-frontier resources confer competitive insulation under contemporary AI, and the polarity-inversion finding (§5) extends the resource-based view diachronically by showing that the era’s dominant capability frontier determines which resource type carries the high-OAI label. The geometry is the durable resource structure; the polarity is its era-contingent valuation.

3.7 External-Indicator Alignment

For the cross-indicator reproduction check (test 8) and the temporal-axis analysis (§5), we projected three external indicators onto the same 1,961-DWA frame as the OAI.

Eloundou task-level labels. Eloundou et al. (2024) released per-task GPT-4 labels assigning each O*NET task to one of five exposure tiers $\{T_0, \dots, T_4\}$. We mapped the tiers linearly to $\{0, 0.25, 0.50, 0.75, 1.0\}$, joined task labels to DWAs via the O*NET 30.2 Tasks to DWAs crosswalk, and computed each DWA’s Eloundou score as the equal-weight mean of its constituent task labels. The result is a DWA-level score that does not share any aggregation step with our OAI. The task-rating data files were originally released with the 2023 arXiv working-paper version (arXiv:2303.10130) of the same work; the formally published version is Eloundou et al. (2024). We retain “Eloundou 2023” as the era-vintage label throughout (era-gradient table in §5, Table 7, Figure 11), where the year marks the vintage of the underlying GPT-4 ratings rather than the publication year of the article.

AIOE. Felten et al. (2021) provide AIOE at the SOC-2018 six-digit occupation level. We mapped each O*NET-SOC code to its parent SOC-2018 (by stripping the two-digit decimal suffix), replicated each SOC-level AIOE value across all DWAs of all occupations sharing that SOC, and took each DWA’s AIOE score as the equal-weight mean across SOC×DWA pairs.

Frey-Osborne. Frey and Osborne (2017) provide the computerisation probability at the SOC-2010 six-digit level for 702 occupations. We obtained the 702-row appendix table directly from the Oxford Martin School working paper PDF (Frey and Osborne, 2013) rather than via downstream compilations, parsed the table programmatically, verified consistency against the compilation embedded in Eloundou et al. (2024) (Spearman $\rho = 1.000$ across 653 matched SOCs), and mapped probabilities to DWAs via the same SOC→OnetSOC→DWA equal-weight aggregation as for AIOE. The direct-from-source pull eliminates the second-hand provenance concern raised by the literature that has used the Eloundou-compiled FO column without re-checking its origin.

Coverage of the 1,961 DWAs is 1,958 (99.85%) for Eloundou, 1,914 (97.6%) for AIOE, and 2,019 (slight over-coverage due to SOC→DWA fan-out) for Frey-Osborne in the macro-level era-inversion analysis. The macro-level era-inversion analysis in §5 additionally uses the 9-group

Table 2: Macro-cluster summary. n -actions counts every micro-action assigned to the macro; % is the share of the 15,817 total. Top-3 TF-IDF terms are computed via the discriminative pooling described in §3.4 (each macro treated as a single document). Dom. stage abbreviations: IC = Intent_Communication, NA = Navigation_Addressing, PD = Perception_Diagnosis, ME = Manipulation_Execution, FV = Feedback_Verification. “Step” is mean `step_order` within the DWA sequence.

Macro	Name	n act.	%	Top-3 TF-IDF	Dom. stage	Cog%	Step
M1	Locating & Provisioning	1,348	8.5%	<i>don, equipment ppe, protective equipment</i>	NA (34%)	35.4%	4.10
M2	Tool-Mediated Physical Execution	1,358	8.6%	<i>inspect, cleaning, fabric</i>	ME (47%)	28.4%	4.98
M3	Iterative Repetition (meta-action)	112	0.7%	<i>repeat steps, repeat, steps remaining</i>	ME (43%)	19.6%	6.99
M4	Diagnostic Analysis	2,585	16.3%	<i>inspect, research, power</i>	PD (31%)	61.8%	4.48
M5	Verification & Stakeholder Reporting	979	6.2%	<i>stakeholders, relevant stakeholders, clarity</i>	FV (39%)	83.0%	5.82
M6	Person-Centered Service Interaction	2,907	18.4%	<i>patient, medical, student</i>	IC (36%)	69.8%	4.54
M7	Planning & Design	891	5.6%	<i>design, develop, review project</i>	ME (33%)	84.2%	3.97
Noise	Generic Action Substrate	5,637	35.6%	—	ME (27%)	61.5%	4.68

partition that splits M4 into its three $K = 12$ sub-macros (M4-HVAC, M4-patrol, M4-data), so that the macro-level rank-correlation has enough variation in mean OAI to be informative.

4 Results: Spatial Axis, Stable Geometry

We organize the spatial-axis results in eight parts: the structure of the action typology (§4.1); evidence that the seven macros differentiate on multiple independent dimensions (§4.2); the bipolar OAI distribution and its resolution-and-equivalence robustness (§4.3); the M4 chimera observation as a self-applied resolution-aggregation diagnosis (§4.4); the intra-cluster bifurcation observed within M2 (§4.5); the generic-action-substrate pattern in the noise group (§4.6); external-indicator reproduction of the bipolar shape (§4.7); and an intelligence-type mechanism that independently predicts OAI (§4.8). The temporal axis is taken up separately in §5.

4.1 The Action Typology

The pipeline described in §3.4 produces seven macros (M1–M7), of which six are domain-thematic and one (M3) is a singleton meta-action layer. Alongside the macros, the HDBSCAN noise label retains 5,637 micro-actions (35.6% of the 15,817 total) as a separate analytical group; at the DWA level, a further `mixed_dwa` group emerges, consisting of the 96 DWAs (4.9% of 1,961) whose largest macro-share falls below the 0.40 dominance threshold (§3.4). The seven macros plus noise account for $10,180 + 5,637 = 15,817$ actions, a complete partition of the dataset. Table 2 reports the action counts, top discriminative TF-IDF terms, dominant process stages, cognitive-physical ratios, and mean `step_order` for every group; we describe each in turn.

M1 (Locating & Provisioning) contains 1,348 micro-actions (8.5% of total) drawn from four micro-clusters (C5, C10, C15, C28). Top discriminative terms are *don, equipment ppe, protective equipment*, indicating a thematic concentration on personal protective equipment and pre-task setup; the dominant process stage is Navigation_Addressing (34%); the cognitive-physical ratio is 35.4%, second only to M2 in physicality.

M2 (Tool-Mediated Physical Execution) contains 1,358 micro-actions (8.6%) drawn from five micro-clusters (C6, C7, C8, C24, C26). Top terms are *inspect, cleaning, fabric*; dominant stage Manipulation_Execution (47%, the highest concentration of any macro on any single

stage); Cog% = 28.4%, the lowest among the seven domain macros and the most physical macro overall.

M3 (Iterative Repetition) is the singleton meta-action layer. It contains 112 actions (0.7%) drawn from a single micro-cluster (C9) whose top terms are *repeat steps*, *repeat*, and *steps remaining*. Its mean `step_order` of 6.99 is the latest in the dataset, reflecting its role as a sequence-tail loop construct. No DWA in the dataset has M3 as its dominant macro; every DWA in which a C9 action appears has it as a minority step. We treat this absence as a structural finding (§4.5), not as a clustering artefact.

M4 (Diagnostic Analysis) is the second-largest macro (2,585 actions, 16.3%) drawn from nine micro-clusters (C2, C12, C16, C17, C19, C20, C25, C33, C34). Top terms *inspect*, *research*, *power*; dominant stage `Perception_Diagnosis` (31%); Cog% = 61.8%, near the population mean.

M5 (Verification & Stakeholder Reporting) contains 979 actions (6.2%) drawn from four micro-clusters (C14, C18, C29, C30); top terms *stakeholders*, *relevant stakeholders*, and *clarity*. Dominant stage `Feedback_Verification` (39%, the highest concentration of any macro on this stage). Cog% = 83.0%, the second-most cognitive macro.

M6 (Person-Centered Service Interaction) is the largest macro (2,907 actions, 18.4%) drawn from seven micro-clusters (C1, C3, C4, C21, C22, C23, C31). Top terms *patient*, *medical*, *student*; dominant stage `Intent_Communication` (36%); Cog% = 69.8%. Note that M6’s discriminative TF-IDF terms span both healthcare and educational interactions; this within-macro heterogeneity reflects the broader *Person-Centered Service Interaction* category encompassing patient, client, customer, and student-facing roles. Both at the action level and at the DWA level (396 DWAs have M6 as dominant), it is the typology’s largest single grouping.

M7 (Planning & Design) contains 891 actions (5.6%) drawn from five micro-clusters (C0, C11, C13, C27, C32). Top terms *design*, *develop*, and *review project*; dominant stage `Manipulation_Execution` (33%) where “manipulation” refers to producing artifacts (specifications, plans, designs) rather than physical objects; Cog% = 84.2%, the highest. Mean `step_order` = 3.97, the earliest position in the workflow.

Generic Action Substrate (Noise) retains 5,637 actions (35.6%) that HDBSCAN refused to assign to any micro-cluster. This is the largest single group in the dataset; we do not assign discriminative top terms in Table 2 because, as we show in §4.6, the noise group has no within-group lexical concentration distinguishable from the population baseline.

mixed_dwa is a DWA-level cell only (no action-level membership): 96 DWAs (4.9%) whose dominant macro-share is below 0.40. These appear in the OAI projection (§4.3) but not in the macro action counts.

Figure 1 plots the 15,817 micro-actions in UMAP-2d, coloured by macro membership. Table 2 and Figure 1 together establish the typology; the next subsection demonstrates that these macros differentiate not only in TF-IDF semantics but along independent process-level and cognitive-physical axes.

4.2 Multi-Dimensional Differentiation

The seven macros separate not only in word usage but synchronously along three independent feature axes: the canonical process stage of each action, the cognitive-physical orientation of the

Semantic Macro-Clusters of 15,817 Occupational Micro-Actions (UMAP 2D)

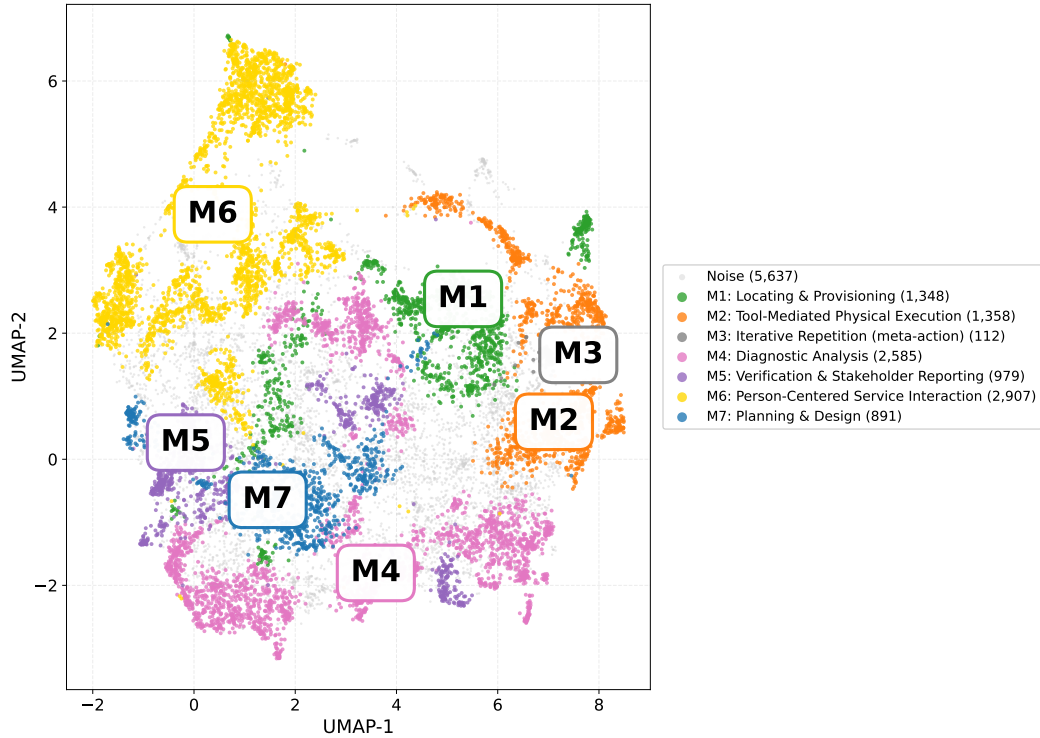


Figure 1: UMAP-2d projection of the 15,817 micro-actions, coloured by K=7 macro assignment. The noise group (light grey, 35.6% of points) is plotted underneath the macro layers.

work, and the typical position of the action within its DWA’s sequence.

Dominant process stage. Each of the five canonical stages is the dominant stage of at least one macro: Navigation_Addressing for M1 (34%), Manipulation_Execution for M2 (47%, the most physical macro), Perception_Diagnosis for M4 (31%), Feedback_Verification for M5 (39%), and Intent_Communication for M6 (36%). M3 and M7 share Manipulation_Execution as their nominal dominant stage (43% and 33% respectively), but the underlying composition is different in kind: M3’s manipulation is meta-procedural (loop-execution actions whose typical text is “repeat steps 4–6”), while M7’s is artifact-producing (writing specifications, drafting plans, generating designs). This distinction collapses into a single label when the stage is read as a coarse five-way category but emerges immediately at the TF-IDF level.

Cognitive-physical orientation. Cog% spans from 19.6% (M3, meta-action) and 28.4% (M2, physical execution) at the physical end to 83.0% (M5) and 84.2% (M7) at the cognitive end, a 64.6 percentage-point range across the seven macros, or 55.8 points if we exclude the meta-action layer. The intermediate macros (M1 at 35.4%, M4 at 61.8%, M6 at 69.8%) trace a graded ascent across the cognitive-physical dimension.

Sequential position in the workflow. The mean `step_order` ranges from 3.97 (M7) to 6.99 (M3), a span of just over three full steps in DWA sequences whose mean length is 8.07. In ascending order: M7 (3.97), M1 (4.10), M4 (4.48), M6 (4.54), Noise (4.68), M2 (4.98), M5 (5.82), M3 (6.99). M7 (Planning & Design) is concentrated at the start of DWAs; M3 (Iterative Repetition) is concentrated near the end, consistent with its loop-construct semantics. M5 (Verification & Stakeholder Reporting) sits late in the sequence (5.82), consistent with its

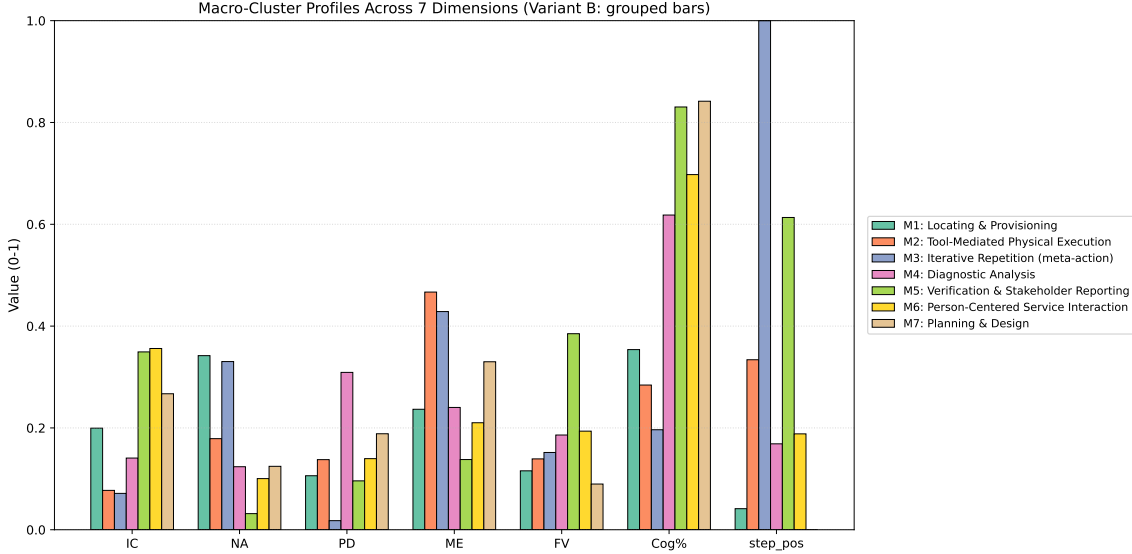


Figure 2: Macro-cluster profiles across seven dimensions: stage shares (IC, NA, PD, ME, FV), cognitive proportion (Cog%), and normalized mean `step_order`. The seven macros differentiate on multiple axes simultaneously.

post-execution review role.

The synchronous differentiation across three independent axes, namely sequential position in the workflow, the canonical process stage, and the cognitive-physical orientation, is structural evidence that the clustering recovers latent structure rather than artifacts of any single feature. A purely cognitive-physical partition would yield a different topology; a purely stage-based partition would yield yet another. The simultaneous coherence across axes constrains the typology to capture something more general than any individual feature. Figure 2 visualizes all three dimensions side by side; the seven macros are simultaneously distinguishable on multiple axes, and no two macros occupy the same cell of the cross-product.

4.3 Bipolar OAI Distribution and Its Robustness

We projected the DWA-level OAI from Gao et al. (2026) onto the eight analysis groups defined in §3.5: M1, M2, M4, M5, M6, M7, Noise, and `mixed_dwa`. Each DWA was assigned to its dominant macro, the macro containing the largest fraction of its micro-actions, with DWAs whose dominant share fell below 0.40 routed instead to `mixed_dwa`. M3 is excluded because no DWA has it as the dominant macro (§4.5 returns to this). The OAI scale is defined on the matrix-discrete set $\{0, 0.3, 0.5, 0.7, 1.0\}$ (§3.5). Group means are continuous because each group averages over many DWAs at different OAI tiers, while the per-DWA values themselves take only the five matrix-permitted levels.

Sample sizes. Group n -DWAs are: M2 = 170, M6 = 396, `mixed_dwa` = 96, Noise = 685, M4 = 324, M1 = 132, M5 = 59, M7 = 99. The smallest group (M5, $n = 59$) is well above the floor for the non-parametric tests we apply. The total n_{DWAs} across the eight projection groups is 1,961, the entirety of the clustered DWA set; no DWA is dropped from the OAI test.

Global test. The Kruskal-Wallis non-parametric ANOVA across the eight groups yields $H = 172.88$ (degrees of freedom = 7), $p = 6.21 \times 10^{-34}$. The null hypothesis that the eight

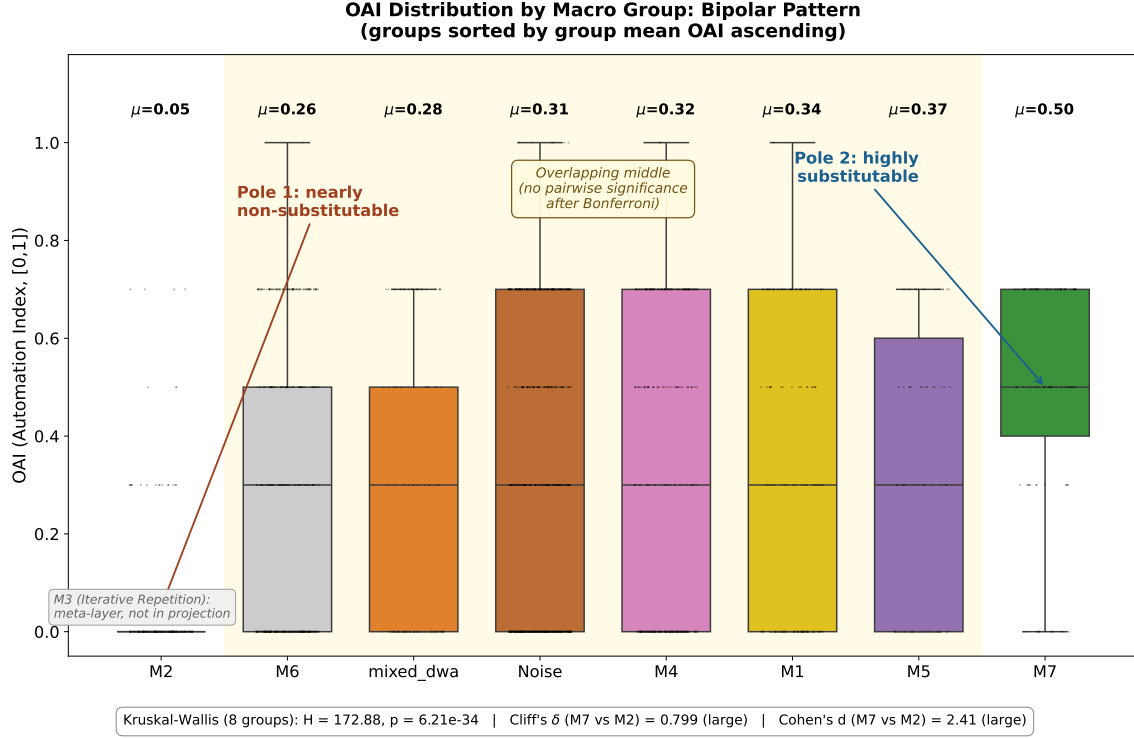


Figure 3: OAI distribution by analysis group, ordered by group median ascending. M2 (left) and M7 (right) occupy the two extremes; the six middle groups (highlighted band) overlap substantially. Bottom panel reports the global test statistic and the M7-vs-M2 effect sizes.

groups share a common OAI distribution is rejected at any conventional threshold; the eight distributions are not interchangeable across the typology.

Group ranking. Figure 3 plots the OAI distributions ordered by group median ascending. Because the OAI scale is discrete, six of the eight groups share the same median value of 0.3, and the median ordering alone does not differentiate them. The group means are unambiguously distinct. Ordered by mean OAI from low to high, the groups are: M2 (0.054), M6 (0.261), *mixed_dwa* (0.282), Noise (0.306), M4 (0.323), M1 (0.342), M5 (0.368), and M7 (0.499). The two endpoints, M2 and M7, occupy positions distinguishable from the rest by a wide margin: M2’s mean is 0.207 below the next-lowest group (M6), and M7’s mean is 0.131 above the next-highest (M5). The remaining six groups cluster within a 0.107-wide band between 0.261 and 0.368, occupying roughly one-tenth of the [0, 1] OAI scale.

Extreme-pair effect sizes. The contrast between M7 and M2 is large by every standard non-parametric and parametric criterion. The Mann-Whitney U test (raw, before Bonferroni correction) returns $U = 15,142$, $p = 3.78 \times 10^{-35}$; after Bonferroni correction across all 28 pairs the corrected p -value remains 1.06×10^{-33} . Cliff’s $\delta = 0.799$ (a non-parametric effect size on $[-1, 1]$, with 0.474 marking the conventional “large” threshold; Romano et al., 2006). Cohen’s $d = 2.41$ exceeds the 0.8 threshold for “large” effect by a factor of three. The mean gap is +0.445 on the [0, 1] OAI scale, roughly the spread between the matrix’s veto value (0) and an automation-expected value (0.5). The three effect-size criteria (Mann-Whitney, Cliff’s δ , Cohen’s d) converge: the polarity is not an artifact of a single test or distributional assumption.

Middle pairwise structure. The pairwise Mann-Whitney comparison with Bonferroni

Table 3: Pairwise OAI Mann-Whitney U tests, Bonferroni-corrected across all $\binom{8}{2} = 28$ pairs. Each cell shows “ \checkmark ” (significant at $p_{\text{Bonf}} < 0.05$) or “ \times ” (not significant), followed by the corrected p -value. **13 of 28 pairs are significant; all 13 involve either M2 or M7.** The remaining 15 pairs trace a band of statistical equivalence among the middle-OAI groups.

	M1	M2	M4	M5	M6	M7	Noise	mixed
M1	—	\checkmark 3.5e−19	\times 1.00	\times 1.00	\times 0.15	\checkmark 3.2e−3	\times 1.00	\times 1.00
M2	\checkmark 3.5e−19	—	\checkmark 1.1e−19	\checkmark 5.4e−18	\checkmark 4.0e−16	\checkmark 1.1e−33	\checkmark 1.6e−22	\checkmark 3.5e−11
M4	\times 1.00	\checkmark 1.1e−19	—	\times 1.00	\times 0.24	\checkmark 1.0e−4	\times 1.00	\times 1.00
M5	\times 1.00	\checkmark 5.4e−18	\times 1.00	—	\times 0.15	\checkmark 4.8e−2	\times 1.00	\times 1.00
M6	\times 0.15	\checkmark 4.0e−16	\times 0.24	\times 0.15	—	\checkmark 1.3e−11	\times 0.54	\times 1.00
M7	\checkmark 3.2e−3	\checkmark 1.1e−33	\checkmark 1.0e−4	\checkmark 4.8e−2	\checkmark 1.3e−11	—	\checkmark 1.1e−7	\checkmark 2.8e−5
Noise	\times 1.00	\checkmark 1.6e−22	\times 1.00	\times 1.00	\times 0.54	\checkmark 1.1e−7	—	\times 1.00
mixed	\times 1.00	\checkmark 3.5e−11	\times 1.00	\times 1.00	\times 1.00	\checkmark 2.8e−5	\times 1.00	—

correction across all $\binom{8}{2} = 28$ pairs is reported in Table 3. Thirteen pairs are significant at $p_{\text{Bonf}} < 0.05$. The 13 significant pairs split as follows: M2 versus each of the other seven groups (seven pairs), plus M7 versus each of the six non-M2 groups (six pairs). *Every one of the 13 significant pairs involves either M2 or M7.* The remaining fifteen pairs are exactly the $\binom{6}{2} = 15$ pairs among the six middle groups (M1, M4, M5, M6, Noise, mixed_dwa). All 15 fail to reject the null at corrected thresholds. The smallest non-significant p_{Bonf} values are 0.15 (M1 vs M6 and M5 vs M6) and 0.24 (M4 vs M6); most other middle-group pairs return $p_{\text{Bonf}} = 1.00$ after correction.

Two-one-sided tests for equivalence within the middle band. Failure to reject the null is not equivalent to evidence for equivalence. We therefore ran TOST on the 15 middle pairs at two pre-registered margins: the primary margin $\delta_d = 0.2 \times \sigma_{\text{pool}} = 0.060$ (corresponding to Cohen’s $d = 0.2$, with σ_{pool} pooled across the six middle groups), and a stricter robustness margin $\delta_{\text{abs}} = \pm 0.05$ on the absolute OAI scale (chosen because it is smaller than the smallest step in the OAI quantisation grid; a $|\Delta_{\text{mean}}|$ below 0.05 cannot move a DWA across an OAI level boundary). The sanity check on the M2 versus M7 extreme pair returns $p_{\text{TOST}} = 1.000$ under both margins, non-equivalent as required, which confirms the setup is valid. On the 15 middle pairs, **only** 1/15 (M4 vs Noise, $p_{\text{TOST}} = 0.020$) reaches equivalence at the primary margin, and 0/15 at the robustness margin. We therefore report the middle as a **low-contrast band rather than a flat plain**. The pairwise tests fail to reject the null, but the equivalence tests likewise fail to confirm absence of contrast. The middle is a gentle gradient, not an absence of gradient.

Resolution sweep across $K = 7, 8, 10, 12, 15$. We re-cut the Ward dendrogram at each resolution, reassigned DWAs, and recomputed the polar means and the middle-pair non-significance rate. The bipolar geometry persists across all five resolutions, but the polar gap widens monotonically rather than collapsing: the low-pole mean OAI moves from 0.055 at $K = 7$ to 0.031 at $K = 12$ and $K = 15$, while the high-pole mean moves from 0.502 to 0.604, expanding the polar gap from 0.45 at $K = 7$ to 0.57 at $K = 12$ and $K = 15$. The middle-pair non-significance rate falls from 100% at $K = 7$ to 61.9% at $K = 8$, 71.4% at $K = 10$, 48.9% at $K = 12$, and 56.4% at $K = 15$, indicating that finer cuts can begin to resolve some middle pairs into distinguishable sub-clusters. Figure 4 visualises both curves; the polar gap grows monotonically as the middle-pair non-significance rate falls. The bipolar shape is therefore

Resolution sweep: bipolar shape sharpens as K grows

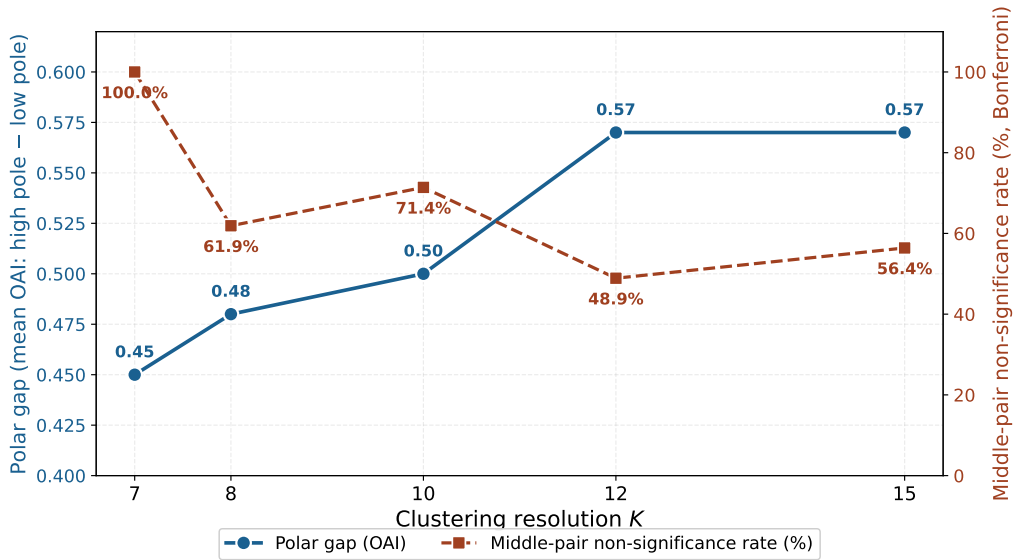


Figure 4: Resolution sweep $K = 7$ to $K = 15$. Left axis: the bipolar polar gap (high-pole mean OAI minus low-pole mean OAI) grows monotonically as the cut becomes finer. Right axis: the middle-pair non-significance rate falls from 100% at $K = 7$ to 48.9% at $K = 12$, then rises slightly to 56.4% at $K = 15$. The bipolar shape is structurally robust to resolution; the middle’s low-contrast band gradually resolves as finer cuts isolate sub-clusters.

robust to resolution; what changes is the resolution of the middle band. The identity of the poles partially reshuffles at $K \geq 10$. At $K = 12$, neither the $K = 7$ M2 nor M7 micro-membership remains in the new low and high poles, because finer cuts isolate sub-portions of $K = 7$ M4 that are even more extreme than $K = 7$ ’s M2 and M7. The bipolar pattern is not a property of M2 and M7 specifically; it is a property of the dendrogram’s two extreme leaves at any resolution.

What “stable geometry” means, and what it does not. The resolution sweep clarifies the precise sense in which the geometry of our title is stable. The stable object is the topological shape: at every resolution we test, the distribution exhibits two extreme poles separated by a large effect-size gap, with a low-contrast middle band between them. This shape does not flatten or collapse as K grows. What is *not* stable is the specific macro labels carried by the poles. Under the headline $K = 7$ cut the poles are labelled M2 and M7; under $K = 12$ they are labelled M4-HVAC and M4-data; future resolutions might surface still finer leaves with the same shape but again different labels. We use the term **stable geometry** to refer to the durable topological container (two poles plus a low-contrast middle) rather than to the durable identity of any specific macro. In the formal account of §6.4, the stable object is the distribution of ω_j vectors across DWAs; which ω_j extremes anchor the poles in a given resolution-and-era pair is contingent. Readers who interpret “stable geometry” as a claim that M2 and M7 themselves are durable across resolutions would mistake the labels for the structure they label.

4.4 The M4 Chimera: A Self-Applied Resolution Diagnosis

The resolution-sweep observation that the polar identities migrate at $K = 12$ invites a direct question: what does $K = 12$ resolve about $K = 7$? We trace the answer to a single macro, M4 (Diagnostic Analysis), which we now identify as a chimera that lexical surface clustering at $K = 7$ holds together under an umbrella its underlying actions do not justify.

At $K = 12$, M4 splits into three sub-macros:

- **M4-HVAC** ($n = 78$ DWAs, mean OAI = 0.031): C33, C34. Top terms *hvac*, *control*, *gas*, *flow*, *temperature*, and *equipment*: physical equipment monitoring.
- **M4-patrol** ($n = 76$ DWAs, mean OAI = 0.114): C2, C12, C19. Top terms *security*, *emergency*, *patrol*, *suspicious*, *situation*, and *evidence*: physical inspection and emergency response.
- **M4-data** ($n = 137$ DWAs, mean OAI = 0.604): C16, C17, C20, C25. Top terms *data*, *accuracy*, *verify*, *dataset*, *completeness*, and *findings*: cognitive data analysis.

The OAI gap from M4-HVAC (0.031) to M4-data (0.604) is 0.573, **larger than the $K = 7$ headline gap of 0.45 between M2 and M7**. M4 was holding together three semantically distinct activities under the umbrella “Diagnostic Analysis” because they share surface lexicon (*inspect*, *examine*, *review*) while differing dramatically in physicality. The same critique we level at AIOE, Eloundou, and FO for aggregating multi-dimensional capability into a single linear scalar (§6.1) applies, in miniature, to our own headline $K = 7$ cut for the M4 cell: lexical similarity has obscured a substantively meaningful sub-structure.

We label this the **M4 chimera** and treat it as a self-applied diagnosis. Three implications follow. First, M4’s homogeneity claim at $K = 7$ is falsified: M4 is not internally homogeneous, but holds two physical sub-clusters plus one cognitive sub-cluster. Second, the bipolar shape is structurally robust. It survives the M4 split, since M4-HVAC takes M2’s polar role and M4-data takes M7’s. The pole-identity claim is not: at finer resolution the poles are M4 sub-clusters, not M2 and M7. Third, the $K = 7$ partition is privileged not because it is unique but because it is the coarsest cut at which the bipolar shape and the dominant-domain semantic labels (Tool-Mediated Physical, Planning & Design) are both legible. Finer cuts reveal more structure; the bipolar shape sharpens, not blurs.

The three other middle macros (M1, M5, M6) do not exhibit the chimera pattern at $K = 12$: M5 and M6 stay as single $K = 12$ blocks (mean OAI of 0.362 and 0.261 respectively), and M1 splits only into a singleton C5-only PPE micro and a main M1 body. The M4 chimera is therefore not a general feature of the middle band; it is a specific structural finding about the Diagnostic-Analysis macro. Figure 5 plots the per-DWA OAI distributions of the three M4 sub-macros side by side; the internal OAI span (0.573) is visibly larger than the headline $K = 7$ M2-vs-M7 gap (0.45) marked by the dotted reference lines.

The M4 chimera as a general lesson for text-similarity-based occupational analysis. Read beyond its specific implications for our $K = 7$ cut, the M4 chimera carries a methodological lesson that applies to a broader class of analyses. Lexical similarity (“inspect,” “examine,” “review”) and substantive similarity (physical embodiment, capital intensity, regulatory exposure,

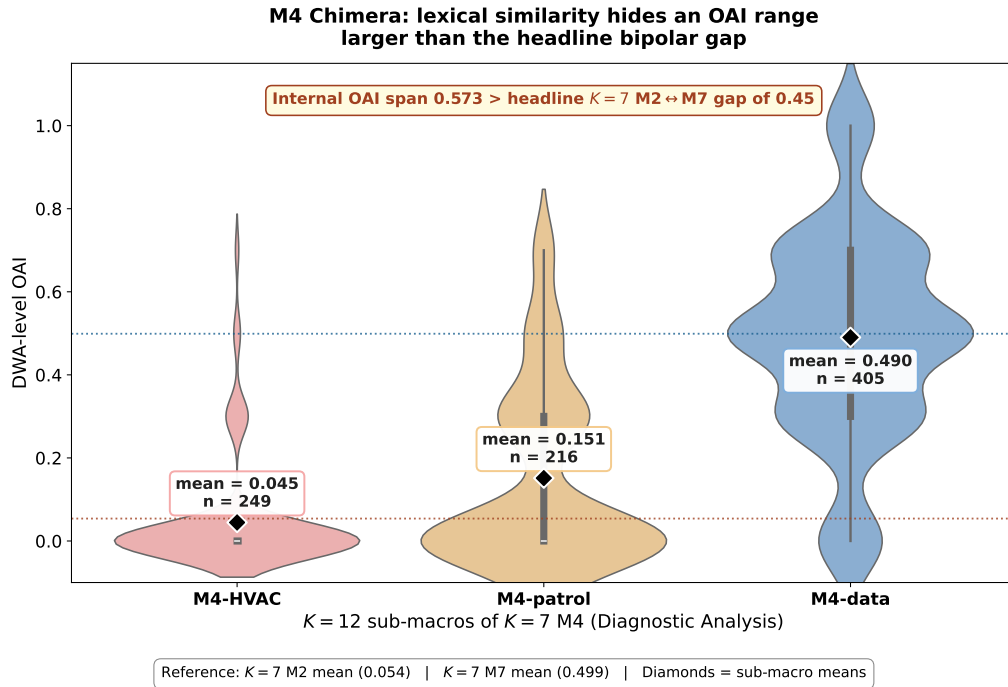


Figure 5: The M4 chimera. $K=7$'s M4 (Diagnostic Analysis) splits at $K = 12$ into three sub-macros whose mean OAI values span from 0.031 (M4-HVAC) to 0.604 (M4-data), a 0.573-wide internal OAI range that exceeds the headline $K = 7$ M2 versus M7 polar gap of 0.45 (dotted reference lines). The lexical similarity holding M4 together at $K = 7$ (*inspect, examine, review*) masks a substantively bipolar substructure between physical equipment monitoring (HVAC, patrol) and cognitive data analysis. Diamonds mark per-sub-macro means.

AI-substitutability) are independent dimensions of occupational text. M4-HVAC and M4-data share surface vocabulary but differ on every dimension that matters economically. This lexical-substantive mismatch is not a defect of our specific encoder, UMAP configuration, or $K = 7$ choice. It is a structural property of how natural-language descriptions of work cluster relative to how work is actually performed, and it generalises to any analytical procedure that rests on text-similarity. Occupational-mobility models built on task-text cosine distance (Deming and Noray, 2020), skill-graph constructions from job postings, topic-modelling of occupational descriptions, and embedding-based occupation classification systems all inherit this risk because they share the same atomic operation: measuring proximity in a semantic space induced by surface text. The remedy is not better embeddings, because an arbitrarily good language model still learns the regularities of how people describe work, not the regularities of how work is performed. The remedy is to validate semantic neighbourhoods against substantive moments computed outside the embedding space, as we do here by cross-referencing the $K = 7$ cut against per-cluster cognitive-physical ratios, dominant process stages, and OAI distributions drawn from an independently calibrated index. Computational labour economics has imported NLP tooling faster than it has imported NLP's known failure modes. The M4 chimera is one such failure mode made concrete, and the validation discipline it forces, triangulating semantic clusters against substantive labour-market moments, should become the default rather than the exception.

4.5 Intra-Cluster Bifurcation within M2

The previous subsection established that M4 holds an internal cognitive-physical split. M2’s OAI mean (0.054) is the lowest in the typology, but its standard deviation (0.147) is the highest among non-mixed groups relative to its mean (coefficient of variation ≈ 2.75 , against an overall CV of 1.03 and an M7 CV of 0.474). Such a high CV at the low end of the OAI scale is unusual: a unimodal distribution clipped near zero typically produces a small CV, since both mean and standard deviation collapse together. M2’s elevated CV instead suggests the variance is distributed across a non-zero secondary mode.

We tested this directly with Hartigan’s dip statistic, a non-parametric test of unimodality. The test on the M2 OAI distribution returns $D = 0.0471$, $p = 7.79 \times 10^{-3}$. The unimodality null is rejected at the 1% level; M2’s OAI distribution is multimodal.

Figure 6 (left panel) plots the M2 overall OAI density, with two visible modes near 0 and near 0.3; the right panel decomposes the macro into its five constituent micro-clusters. Sorted by per-micro mean OAI, the five micros split into two clearly separated bands:

- C26 (*using, inspect, workpiece*): mean OAI = 0.017, $n = 72$ DWAs;
- C24 (*fabric, pieces, garment*): mean OAI = 0.023, $n = 13$ DWAs;
- C8 (*cleaning, clean, area*): mean OAI = 0.026, $n = 43$ DWAs;
- C6 (*sample, ingredients, container*): mean OAI = 0.121, $n = 24$ DWAs;
- C7 (*kitchen, dishes, food*): mean OAI = 0.200, $n = 18$ DWAs.

The first three micros (C26, C24, C8) cluster tightly in the [0.017, 0.026] interval; the fourth and fifth (C6, C7) sit roughly an order of magnitude higher, in the [0.121, 0.200] interval. The within-band variance is small in each of the two bands; the between-band gap is approximately 0.1 on the OAI scale. The two modes can be characterised post-hoc as a structured-manufacturing cluster (C26 workpiece machining, C24 fabric and garment work, C8 surface cleaning) versus a less-structured manual-work cluster (C6 sample preparation and C7 food-service work); we reserve theoretical interpretation for §6. Within §4, the finding is restricted to its statistical content: the M2 macro, which appears as a single low-OAI extreme in the bipolar plot, is internally bifurcated into two non-overlapping bands.

4.6 The Generic Action Substrate

The bipolar result of §4.3 situates the noise group at OAI mean 0.306, squarely in the middle band and statistically equivalent to every other middle-group macro after Bonferroni correction. We now ask whether the noise group is *distinct from the population in any measurable way*, on any of the four feature axes available to us.

The answer is no on each axis. The noise group’s distribution of `mapped_stage` is within 1.2 percentage points of the full-population distribution on every stage: Manipulation_Execution 27.1% vs full 26.5%; Intent_Communication 21.4% vs 22.5%; Feedback_Verification 20.5% vs 19.1%; Perception_Diagnosis 16.7% vs 17.3%; Navigation_Addresssing 14.3% vs 14.6%. The cognitive-physical split is 61.5% Cognitive vs 60.3% in the full population, a 1.2 percentage-point difference. Mean `step_order` is 4.68 vs 4.64 across the full population, a 0.04-step difference

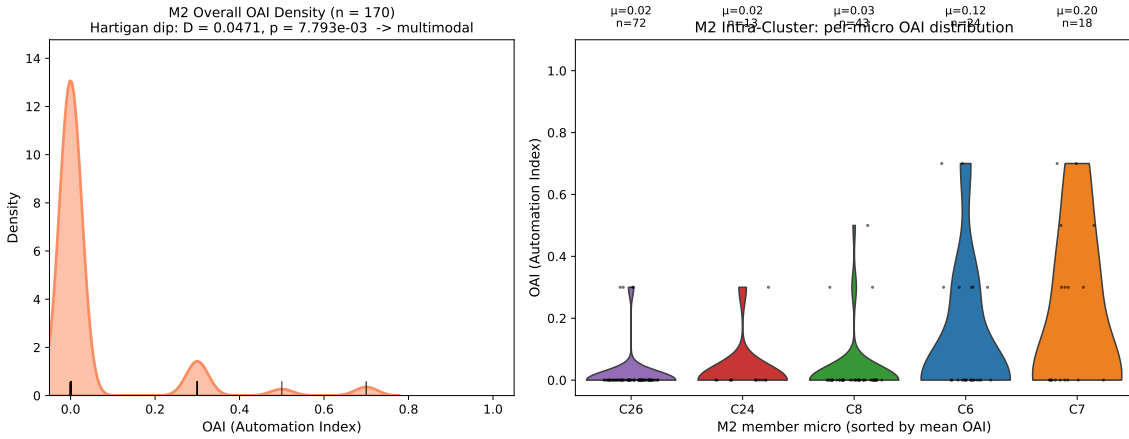


Figure 6: M2 intra-cluster heterogeneity. **Left:** overall OAI density for M2 with Hartigan dip statistic. **Right:** per-micro OAI distributions sorted by mean.

Table 4: External-validity statistical summary. The Kruskal-Wallis test rejects the global null at the 10^{-33} level. The M7-vs-M2 contrast yields large effects on both non-parametric (Cliff’s δ) and parametric (Cohen’s d) criteria. Hartigan’s dip rejects unimodality of M2’s OAI distribution; the two-sample Kolmogorov-Smirnov test fails to reject the null that the noise group’s OAI distribution is identical to the full population.

Test	Statistic	p -value	Effect size	Interpretation
Kruskal-Wallis (8 groups)	$H = 172.88$	6.21×10^{-34}	—	Strong overall difference.
M7 vs M2, Mann-Whitney U	$U = 15,142$	3.78×10^{-35}	Cliff’s $\delta = 0.799$	Large effect ($ \delta > 0.474$).
M7 vs M2, Cohen’s d	$d = 2.41$	—	$d = 2.41$	Large effect ($ d > 0.8$).
Hartigan dip (M2 OAI)	$D = 0.0471$	7.79×10^{-3}	—	Multimodal ($p < 0.05$).
KS (Noise vs full pop.)	$D = 0.0267$	0.851	—	Indistinguishable.

and less than 1% of the typical 5 to 13 step DWA range. On the OAI axis itself, the two-sample Kolmogorov-Smirnov test returns $D = 0.0267$, $p = 0.851$: the null hypothesis that the noise-group OAI distribution and the full-population OAI distribution are drawn from the same underlying distribution cannot be rejected at any conventional significance level. The same KS test performed on M2’s OAI versus the full-population OAI gives a much larger D statistic and rejects the null at $p < 10^{-30}$, consistent with M2’s bipolar-extreme position.

We interpret this convergent indistinguishability across four dimensions, namely stage, cognitive-physical orientation, sequential position, and OAI, as a structural feature of the dataset. Roughly one-third of occupational micro-actions are domain-neutral generic verbs whose distributions in stage, cognitive-physical content, sequence position, and substitutability all reproduce the population shape. Theoretical implications are taken up in §6.

4.7 External-Indicator Reproduction

The bipolar shape we report could in principle be an artifact of the OAI calibration itself. To rule out this circularity, we project three external indicators, computed entirely outside our pipeline, onto the same 1,961-DWA frame and ask whether the bipolar shape reproduces. Indicator alignment is described in §3.7.

Eloundou GPT-4 task labels. The cleanest cross-method check uses the per-task GPT-4 exposure labels from Eloundou et al. (2024), projected to DWAs by equal-weight task averaging. The Kruskal-Wallis test across the eight macro groups yields $H = 298.4$, $p = 1.32 \times 10^{-60}$. The M2 versus M7 extreme pair returns Cliff’s $\delta = 0.902$ (Cohen’s $d = 2.98$), *larger* than the $\delta = 0.799$ obtained under our OAI. M2 again sits at the low pole (mean Eloundou exposure 0.083, median 0); M7 at the high pole (mean 0.496, median 0.50). The six middle macros yield 12 of 15 non-significant pairs after Bonferroni correction, closely tracking our OAI’s 15 of 15. The bipolar shape reproduces under a completely different rating procedure. At the DWA level, OAI and Eloundou’s task labels correlate at Spearman $\rho = 0.635$ ($p = 8 \times 10^{-222}$, $n = 1,958$); two methodologically independent procedures agree on the substitutability ordering of nearly every DWA in the dataset.

AIOE. Felten et al.’s AIOE, derived from ability-rating crowd estimates rather than from task-level GPT prompting, returns Kruskal-Wallis $H = 287.4$ ($p = 3.0 \times 10^{-58}$) across the eight macros. The M2 versus M7 contrast remains the largest pair, but the polar identity differs: AIOE places M4-data at the high pole (mean AIOE 0.89) and M2 at the low pole (mean AIOE -0.79). Eighteen pairs are Bonferroni-significant, against 13 for our OAI. The bipolar structural form (a low pole, a high pole, and a middle band) reproduces; the middle is less indistinguishable under AIOE, partly because of AIOE’s higher continuous resolution (ability-weighted linear sums rather than five discrete OAI tiers). DWA-level Spearman with OAI is 0.447.

Frey-Osborne. Frey-Osborne computerisation probability, projected to DWAs via $\text{SOC} \rightarrow \text{OnetSOC} \rightarrow \text{DWA}$ equal-weight mean (§3.7), returns Kruskal-Wallis $H = 329.0$ ($p = 3.9 \times 10^{-67}$). Nineteen pairs are Bonferroni-significant. The M2 versus M7 contrast under FO is *inverted relative to OAI*: M2 sits near the FO high pole (mean FO probability 0.70) and M7 sits near the FO low pole (mean FO 0.29). This sign reversal is the subject of §5. For the present subsection we note only that the bipolar structural form (two extremes plus a middle band) reproduces under FO as well. DWA-level Spearman between FO and OAI is $\rho = -0.116$ ($p = 5 \times 10^{-7}$), consistent with the macro-level polarity inversion.

Synthesis. Three indicators computed entirely outside our OAI pipeline, each using a different aggregation rule, a different rating source, and a different vintage, all yield a bipolar shape with a low pole, a high pole, and a middle band when projected onto our action-level macro typology. The structural form of the bipolar pattern is robust to indicator choice; the polar content is contingent on the indicator’s era and rating procedure. This eliminates the circularity concern that the bipolar shape is an artifact of OAI’s specific quantisation grid. The same shape emerges under the continuous-valued AIOE and the binary-derived FO probability. The shape lives in the action-level typology, not in the rating instrument. Figure 7 visualises the four indicators side by side on the same eight macros; Figure 8 reports the underlying DWA-level OAI versus Eloundou scatter.

4.8 Intelligence-Type Mechanism

The bipolar shape begs a mechanistic question: *why* are M2 and M7 the poles, and why do the middle macros refuse to be ordered? We address this through the four-way intelligence-type classification described in §3.6, in which each action is labelled Linguistic, Multimodal Perception,

Bipolar reproduction under four independent exposure indicators

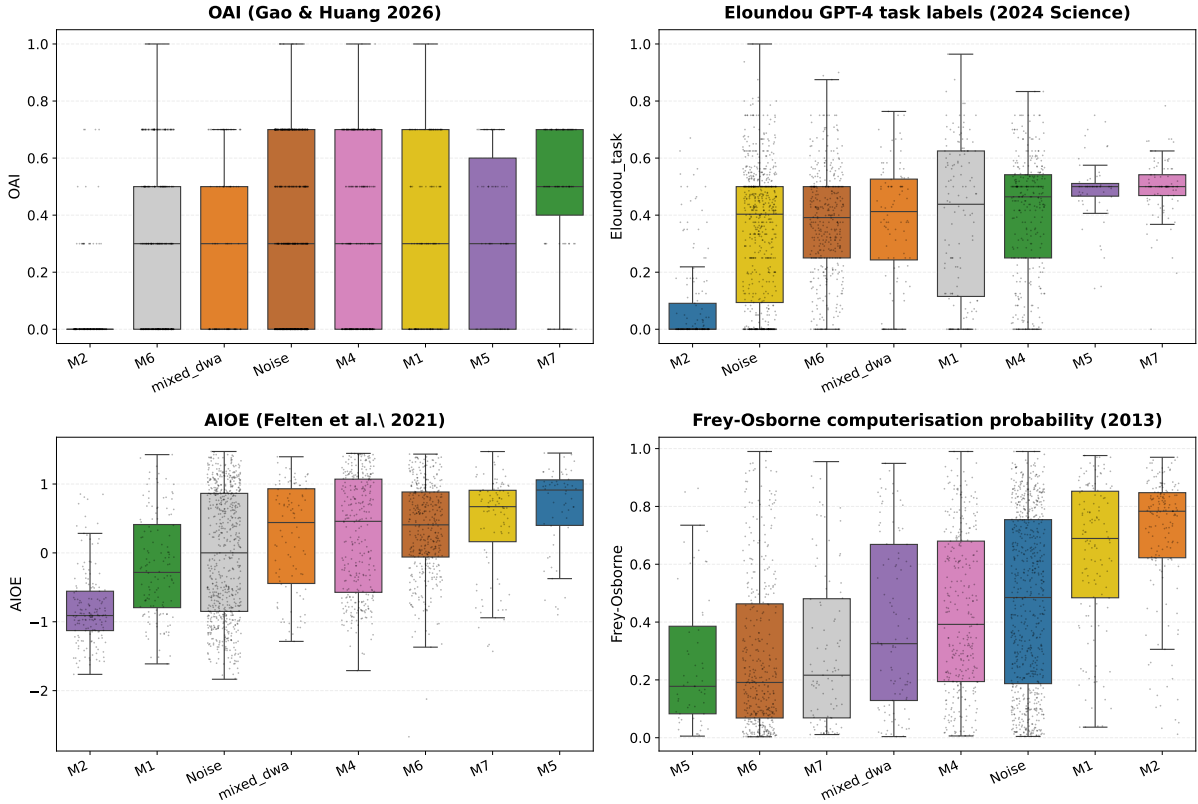


Figure 7: Bipolar reproduction under four independent exposure indicators. Each panel plots the DWA-level distribution of one indicator across the eight macro groups, with M2 and M7 (or their equivalent extremes) anchoring the polar positions. The bipolar shape is visible under all four indicators; what changes is which pole is high (compare OAI and Eloundou with Frey-Osborne).

Embodied, or Human-Bound based on prototype-anchored cosine similarity under BGE encoding. The classification is independent of the macro structure, since it depends on action text and prototype geometry alone, and therefore provides a non-circular mechanism check.

Overall class distribution across the 15,817 actions: Linguistic 49.8%, Multimodal Perception 20.5%, Embodied 16.4%, Human-Bound 13.3% (median classifier confidence 0.597). The four classes are intelligible categories of contemporary AI capability: Linguistic actions are tasks LLMs perform well (drafting, summarising, computing-over-text); Multimodal Perception actions are tasks contemporary vision-language models address with rapidly-rising competence; Embodied actions require physical manipulation; Human-Bound actions require interpersonal trust or legal accountability.

Cross-tab by macro. Table 5 reports the share of each intelligence type within each $K = 7$ macro. The two polar macros are concentrated in opposite intelligence types: M2 is 56% Embodied and 27% Multimodal Perception, with only 15% Linguistic content; M7 is 95% Linguistic with 1% Multimodal Perception, 3% Embodied, and 2% Human-Bound. M6 (Person-Centered Service) is split between Linguistic (41%) and Human-Bound (43%). Within M4 the chimera (§4.4) is recapitulated in intelligence-type composition: M4-HVAC is 83% Multimodal Perception, M4-patrol is 37% Linguistic / 30% Multimodal Perception / 23% Human-Bound,

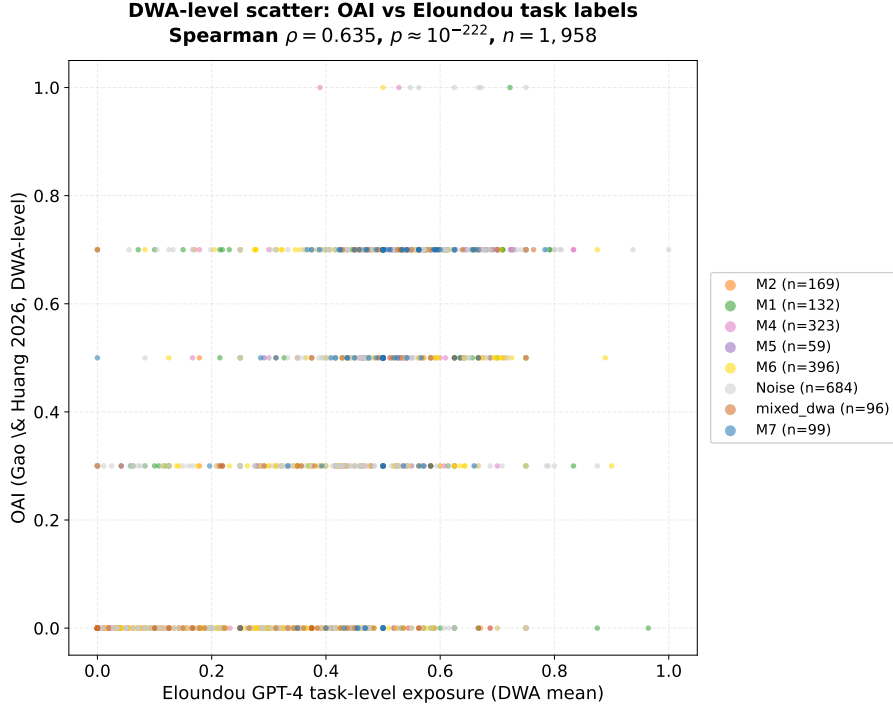


Figure 8: DWA-level scatter between our OAI and Eloundou’s GPT-4 task-rating exposure ($n = 1,958$ DWAs after alignment, Spearman $\rho = 0.635$, $p \approx 10^{-222}$). Two methodologically independent procedures, Tech-Risk Bottleneck aggregation (Gao et al., 2026) and per-task GPT-4 prompting (Eloundou et al., 2024), agree closely on the DWA-level substitutability ordering, breaking the circularity worry that the bipolar shape might be an OAI quantisation artifact.

and M4-data is 87% Linguistic.

Figure 9 reproduces the cross-tab as a heatmap with the M4 sub-macros split out, making the chimera (§4.4) visible at intelligence-type resolution: M4-HVAC concentrates in Multimodal Perception (83%), M4-patrol mixes Linguistic and Human-Bound, and M4-data is overwhelmingly Linguistic (87%).

Intelligence type predicts OAI. If the intelligence-type layer is interpretive rather than tautological, it should predict OAI independently. We assigned each DWA the modal intelligence type of its actions, retaining the full 1,961-DWA frame. This is a different grouping operation from the macro-dominance assignment in §4.3: every DWA is here re-partitioned into one of four intelligence types regardless of macro membership, so the per-class n here and the per-macro n in §4.3 are not directly comparable. We then tested OAI distributions across the four types. The four classes are highly distinguishable on OAI: Linguistic $n = 1,070$ DWAs, mean OAI = 0.427 (median 0.5); Human-Bound $n = 238$, mean OAI = 0.219; Multimodal Perception $n = 331$, mean OAI = 0.125; Embodied $n = 322$, mean OAI = 0.060. The Kruskal-Wallis test returns $H = 527.6$ ($p = 4.87 \times 10^{-114}$) across the four classes, a stronger signal than the macro-level $H = 172.9$, despite using a four-way rather than eight-way partition. Pairwise Mann-Whitney with Bonferroni correction returns **all six pairs significant** at $p_{\text{Bonf}} < 10^{-4}$, with the Linguistic-versus-Embodied contrast at $p_{\text{Bonf}} = 1.76 \times 10^{-77}$. The LLM-class OAI lead is $3.37\times$ the mean of the other three classes combined. Figure 10 plots the per-class OAI distributions side by side.

Table 5: Intelligence-type composition by macro (BGE labels, row-normalised %). The two poles concentrate in opposite intelligence types: M2 is Embodied-dominant, M7 is Linguistic-dominant. M6 mixes Linguistic and Human-Bound. The M4 sub-macros (§4.4) recapitulate the M4 chimera: M4-HVAC concentrates in Multimodal Perception, M4-data in Linguistic.

Macro	Linguistic	Mm. Perception	Embodied	Human-Bound
M1 (Locating)	31%	17%	47%	5%
M2 (Tool-Mediated)	15%	27%	56%	2%
M3 (Iterative Repetition)	61%	6%	33%	0%
M4 (Diagnostic)	52%	37%	5%	7%
M5 (Verification)	89%	7%	1%	4%
M6 (Person-Centred Service)	41%	10%	6%	43%
M7 (Planning & Design)	95%	1%	3%	2%
Noise	53%	24%	15%	9%

The bipolar shape recovered. The intelligence-type pattern recovers the bipolar shape from a different angle: M7’s 95% Linguistic composition aligns it with the Linguistic class’s OAI mean of 0.427, while M2’s 56% Embodied composition aligns it with the Embodied class’s OAI mean of 0.060. The poles are not arbitrary macros at the OAI extremes; they are the macros whose intelligence-type composition aligns with the highest- and lowest-OAI intelligence types respectively. The middle macros are mixed in composition (M6, for instance, is 41% Linguistic and 43% Human-Bound), which is structurally what middle aggregate OAI scores look like at the action level. The middle band is statistically low-contrast because it is a mixture in intelligence-type composition.

This mechanism leads directly into the temporal axis in §5: if the polarity is mediated by which intelligence type aligns to which automation-friendly capability frontier, and if the dominant frontier moves across time, then the polarity itself should move with it. We show next that it does.

5 Results: Temporal Axis, Polarity Inversion

The spatial-axis results in §4 establish that the bipolar shape is robust across resolution, encoder, and indicator. The natural next question is whether the polarity itself, that is, which macros sit at the high pole and which at the low, is similarly robust across the temporal dimension. Three exposure indicators in our alignment set span thirteen years of AI capability evolution: Frey-Osborne’s 2013 computerisation probability, Felten et al.’s 2018 and 2021 AIOE, Eloundou et al.’s 2023 GPT-4 task labels, and our own 2026 OAI. We use this span to ask whether the polar ordering is structurally stable or temporally contingent. The answer drives the second main finding of this paper.

5.1 Era Gradient as a Preliminary Observation

As preamble to the polar-reversal analysis, we report a single descriptive observation. For each indicator, projected onto the eight $K = 7$ macro groups, we count the fraction of middle-group pairs (the six pairs among M1, M4, M5, M6, Noise, mixed_dwa, giving $\binom{6}{2} = 15$ pairs) that are non-significant after Bonferroni correction. Older indicators with broader rating coverage are

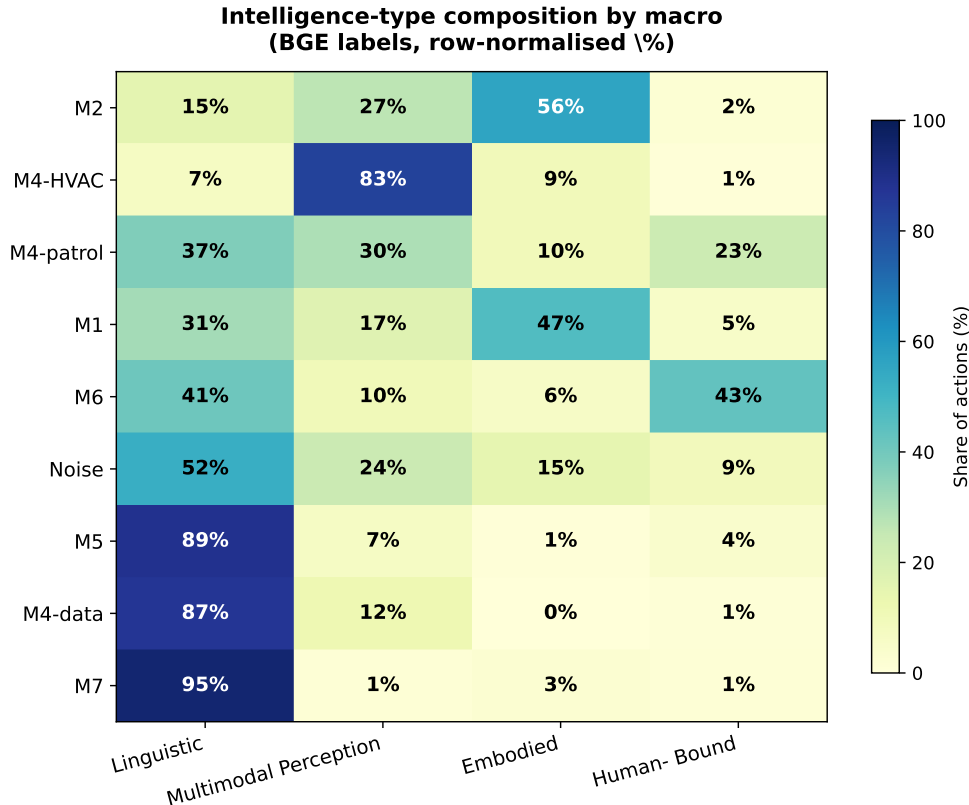


Figure 9: Intelligence-type composition by macro (BGE labels, row-normalised %, with M4 split into $K=12$ sub-macros). M2 is dominated by Embodied; M7 by Linguistic; M4-HVAC by Multimodal Perception; M4-data by Linguistic; M6 mixes Linguistic and Human-Bound. The polar identity of each macro is closely tracked by the intelligence-type composition.

expected to make more middle pairs significant (resolving more contrast); newer LLM-rating indicators are expected to flatten the middle into a low-contrast band.

Table 6: Middle-pair non-significance rate by indicator vintage. The qualitative trend is monotone increasing across the four indicators. With $n = 4$ indicators no formal trend test is supported; we report the ordering as a descriptive observation only.

Indicator	Year	Middle non-sig
Frey-Osborne computerisation probability	2013	5/15 (33%)
Felten et al. AIOE	2018	6/15 (40%)
Eloundou et al. task labels	2023	12/15 (80%)
Our OAI	2026	15/15 (100%)

Table 6 shows a monotone increase in middle-pair non-significance from 33% at the 2013 indicator to 100% at the 2026 indicator. With $n = 4$ indicators no formal trend test is supported; we report the ordering as a descriptive setup observation only. The substantive temporal finding is the polarity inversion in §5.2 below.

5.2 Polarity Inversion

For this analysis we use the 9-group partition that splits M4 into its three $K = 12$ sub-macros (M4-HVAC, M4-patrol, M4-data), giving macro-level rank correlation enough variation to be

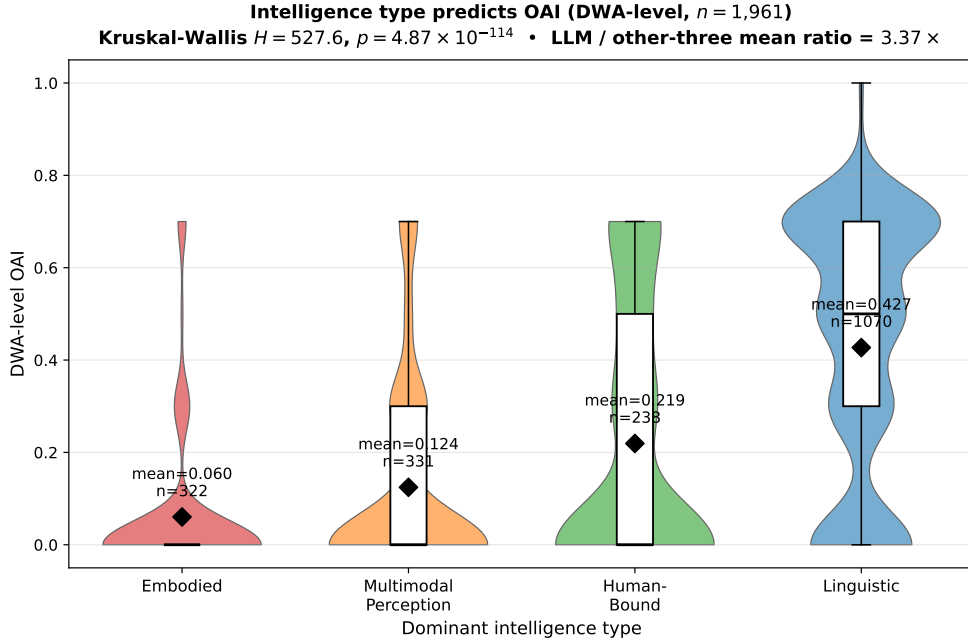


Figure 10: DWA-level OAI distribution by dominant intelligence type ($n = 1,961$ DWAs total). Linguistic-dominant DWAs (the rightmost violin) have mean OAI 0.427, $3.37\times$ the mean across the other three classes combined (0.127). The four-way partition produces a stronger global signal ($H = 527.6$) than the eight-way macro partition ($H = 172.9$, §4.3), and all six pairwise contrasts reach Bonferroni significance.

informative. This is the only place in the paper where we depart from the $K = 7$ 8-group partition; the rationale is that the macro-level rank correlation across only 8 distinct points would be both noisier and less interpretable, given that the M4 chimera (§4.4) holds three distinct OAI tiers within a single $K = 7$ cell. The temporal-inversion claim is presented with this 9-group framing throughout.

Per-macro mean exposure, 2013 to 2026. Table 7 reports each macro’s mean exposure under each indicator. The story is visible row by row. M2 (Tool-Mediated Physical), the high-exposure pole under FO in 2013 with mean probability 0.703, drops to mean OAI 0.058 in 2026, a 0.65-unit drop on the $[0, 1]$ scale, larger than $K = 7$ ’s entire polar gap. M4-HVAC, with mean FO 0.654, drops to mean OAI 0.035. M7 (Planning & Design), low-exposure under FO with mean 0.287, rises to mean OAI 0.504. M4-data, with mean FO 0.340, rises to mean OAI 0.601. The four largest movers are exactly the four poles, two from each direction, which suggests that the inversion is concentrated at the poles rather than distributed evenly across the typology. The middle macros (M1, M5, M6, Noise) shift only slightly and remain mid-OAI in both eras.

Macro-level rank-correlation tests. Table 8 reports Spearman rank correlations across the 9 macros between FO and each LLM-era indicator. FO is negatively correlated with both OAI ($\rho = -0.650$, $p = 0.058$) and the Eloundou GPT-4 task labels ($\rho = -0.750$, $p = 0.020$). The FO \leftrightarrow Eloundou correlation reaches significance at the 0.05 level. With only $n = 9$ macros, statistical power is limited; the substantive content is in the sign and the magnitude. A negative Spearman of -0.75 across 9 macros indicates that the polar ordering under FO is the near-mirror-image of the polar ordering under Eloundou.

Table 7: Per-macro mean exposure under the four indicators (9-group $K = 12$ partition; M4 split into HVAC / patrol / data). Macros are ordered by mean OAI ascending. The first four rows (M2, M4-HVAC, M4-patrol, M1) flip from FO high-risk to OAI low-exposure; the last four (M5, M4-data, M7, with M6 mid-table) move the opposite way. Frey-Osborne values are computed from the official Oxford Martin appendix (Frey and Osborne, 2013), verified against Eloundou et al. (2024) compilation at Spearman $\rho = 1.000$ across 653 matched SOC codes (§3.7).

Macro	Mean OAI	Mean Eloundou	Mean AIOE	Mean FO
M2 (Tool-Mediated)	0.058	0.086	-0.787	0.703
M4-HVAC	0.035	0.214	-0.601	0.654
M4-patrol	0.132	0.357	0.112	0.388
M1 (Locating)	0.345	0.387	-0.192	0.626
M6 (Person-Centred Service)	0.262	0.380	0.357	0.300
Noise	0.300	0.340	-0.008	0.471
M5 (Verification)	0.350	0.464	0.574	0.306
M4-data	0.601	0.543	0.890	0.340
M7 (Planning & Design)	0.504	0.497	0.469	0.287

Table 8: Macro-level Spearman correlations between Frey-Osborne (2013) and the LLM-era indicators. The negative signs and substantial magnitudes establish the polar reversal. The within-FO check (old Eloundou-compiled column vs Oxford Martin original) returns $\rho = 0.983$, confirming the inversion is not driven by FO-source choice.

Macro-level rank correlation ($n = 9$ macros)	Spearman ρ	p -value
FO (Oxford Martin original) \leftrightarrow OAI 2026	-0.650	0.058
FO (Oxford Martin original) \leftrightarrow Eloundou 2023	-0.750	0.020
FO Eloundou-compiled column \leftrightarrow FO Oxford Martin	+0.983	1.9×10^{-6}

Within-FO sanity check. Before reading the inversion as substantive, we verified that the FO macro-level means are stable across the two available FO sources. The compilation of FO computerisation probabilities embedded in Eloundou et al. (2024) `autoScores.csv` (the second-hand version used by some downstream papers) reproduces the original Oxford Martin appendix (Frey and Osborne, 2013) at Spearman $\rho = 1.000$ across 653 matched SOC codes (mean absolute difference < 0.001 , max < 0.001). The 9-group macro-level Spearman between the two FO versions is $\rho = 0.983$ ($p = 1.9 \times 10^{-6}$). The polar reversal does not depend on FO-source choice; we report the Oxford Martin original throughout for provenance clarity, and the Eloundou compilation yields the same result.

DWA-level corroboration in the full $n = 1,958$ sample. The macro-level rank correlations above are computed across only $n = 9$ macros, which limits statistical power even though the sign and magnitude of the inversion are large. To corroborate the inversion in the full sample space, we computed the DWA-level Spearman rank correlation between Frey-Osborne’s 2013 computerisation probability and our 2026 OAI across all aligned DWAs. The result is $\rho = -0.116$ ($p = 5 \times 10^{-7}$, $n = 1,958$). The absolute magnitude is necessarily smaller than the macro-level $\rho = -0.650$ because the OAI is concentrated on the five-point discrete set $\{0, 0.3, 0.5, 0.7, 1.0\}$ while FO is continuous on $[0, 1]$, and because the noise group and middle macros contribute substantial within-class variation that washes out cross-DWA rank order. The substantive content is the negative sign of the correlation across a $n = 1,958$ sample, which establishes the polarity inversion as a statistically robust finding independent of the macro-level

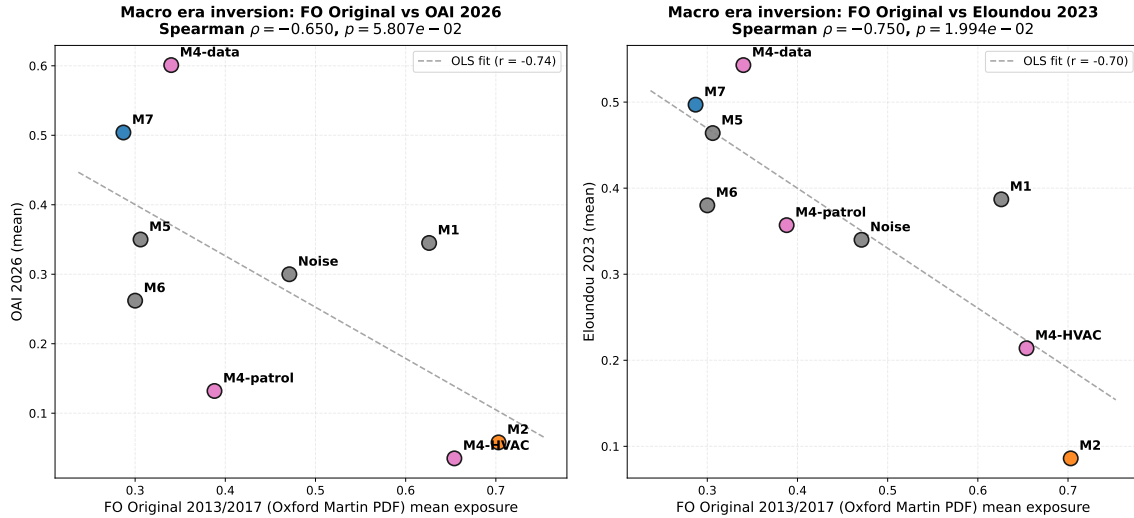


Figure 11: Polar reversal at the macro level. **Left:** mean FO (2013, Oxford Martin original) on the x -axis vs mean OAI (2026) on the y -axis; the OLS regression slopes downward, with Spearman $\rho = -0.650$. **Right:** same plot against Eloundou’s 2023 task labels; the inversion is stronger, with Spearman $\rho = -0.750$. M2 and M4-HVAC (the high-FO, low-LLM-era macros) and M7 and M4-data (the low-FO, high-LLM-era macros) anchor the inverse relationship.

partition: the p -value of 5×10^{-7} in the large sample is roughly five orders of magnitude smaller than the p -value of 0.020 in the macro-level test, so the inversion does not rest on the eight or nine extreme leaves of the dendrogram alone. The same DWA-level test against Eloundou’s 2023 task labels yields $\rho = +0.635$ ($p \approx 10^{-222}$, $n = 1,958$), confirming that the LLM-era indicators OAI and Eloundou rank DWAs concordantly while FO ranks them in approximately reversed order.

Rank-level reversal at the poles. The substantive content of the negative Spearman is the rank-level reversal at the poles, the **reversing poles** of our title made concrete. Under FO, M2 ranks 9th of 9 (highest exposure); under OAI it ranks 2nd of 9. Under FO, M7 ranks 2nd (low exposure); under OAI it ranks 8th (high). M4-HVAC moves from rank 8 (FO) to rank 1 (OAI); M4-data moves from rank 4 to rank 9. The four largest-movers each shift by 5 to 7 rank positions out of a possible 8. The bipolar shape persists, but the labels on the poles swap.

5.3 Geometry vs Content: Synthesis

The spatial-axis results in §4.3 through §4.8 document that the bipolar geometry is robust to three sources of methodological variation: clustering resolution ($K = 7$ to $K = 15$, polar gap widens), encoder family (MPNet to BGE), and exposure indicator (OAI, Eloundou, AIOE, FO all produce two poles plus a middle). The temporal-axis result in §5.2 documents that the polarity content, that is, which macros sit at which pole, is not robust to indicator vintage. The 2013 computerisation-probability arrangement places physical-tool execution at the high pole and planning at the low; the 2023 LLM-era arrangement reverses this.

The two findings are not in tension; together they characterise the structural object that is stable. The bipolar shape is the geometry of occupational substitutability: there exists a high pole, a low pole, and a low-contrast middle band, at all clustering resolutions tested and under

all four exposure indicators we examined. The **reversing poles** between FO 2013 and our 2026 OAI are the content of those poles; the bipolar shape itself is the container in which the reversal occurs. Content is contingent on the era’s dominant AI-capability frontier; the container is not. In 2013, the engineering-bottleneck reading of automation pointed at physical-tool execution as the next frontier and at cognitive planning as the most-protected from automation. In 2023 to 2026, the LLM-rating procedure points the opposite way: cognitive Linguistic actions are the LLM-frontier and physical execution is the most-protected. The mechanism in §4.8, namely the four-way intelligence-type classification in which the Linguistic class has $3.37\times$ the mean OAI of the other three classes, supplies the causal reading. The era’s dominant capability is what determines which intelligence type maps to the high-OAI pole. The geometry is invariant; the labels on the poles are not.

This characterisation has a sharp implication for the consulting forecasts surveyed in §2.4: a single-point exposure projection inherits the era’s capability frontier. If the frontier moves, and the FO \rightarrow Eloundou rank-correlation result indicates it has moved decisively in one direction over a single decade, then any contemporaneous projection is provisional at best. What survives the frontier movement, and what we therefore propose as the structurally robust object of empirical interest, is the **stable geometry**: the count of poles (two), the existence of a low-contrast middle band, and the intelligence-type composition that drives polar identity. These structural properties are what a future-of-work analysis can transport across capability eras; the per-macro exposure score itself cannot.

6 Discussion

6.1 From Gradient to Polarity

What the OAI measures, and what it does not. Before discussing the substantive findings, we make explicit a definitional commitment that is implicit throughout the paper. The Occupational Automation Index we project is a measure of *task-level exposure* to AI capability, not a forecast of *job-level displacement*. High OAI on a macro indicates that the constituent micro-actions are technically and risk-tolerably executable by contemporary AI; it does not entail that the occupations dominated by that macro will lose employment. The distinction is the substitution-vs-augmentation asymmetry that the recent task-based literature (Acemoglu and Restrepo, 2022, 2018) has placed at the centre of automation theory: exposed actions can be *substituted* (the AI replaces the worker on the action) or *augmented* (the AI complements the worker, raising productivity per worker without reducing employment). Programmers exposed to GitHub Copilot are a canonical augmentation case: their tasks are high-OAI on every reasonable index, but employment in software development has not contracted, and per-worker output has expanded. The bipolar structure documented here is a structure of exposure; whether each pole’s exposure resolves into substitution or augmentation depends on factors outside our index, including organisational adoption choices, labour-market institutions, and the marginal value of expanded per-worker output in the affected occupations. We return to this distinction in §6.7 (Proposition 4) and treat it as a stated limitation of the index in §6.8.

The central spatial-axis claim of this paper is that the continuous-gradient assumption

embedded in modern AI-substitutability research is an aggregation artifact rather than a property of the underlying data. When the AIOE, the Frey-Osborne risk, the Eloundou E_1/E_2 , and similar indices are computed by linearly summing capability ratings across many ability or task dimensions, the central limit theorem all but guarantees that the resulting score will populate a smooth interval: averaging many discrete components produces a near-continuous distribution at the aggregate level even when the components themselves are discrete or polarised. The continuity of the score is therefore not informative about the underlying micro-structure; it is structurally inherited from the aggregation rule. Once we cluster at the action level and project the OAI onto the resulting typology without further aggregation, the continuity collapses: two extreme macros separated by a Cohen’s d of 2.41 anchor the distribution, and a six-macro low-contrast middle band sits between them.

This finding stacks directly on the contribution of Gao et al. (2026). There, we showed that the Bottleneck (Leontief-style) aggregation of Tech and Risk factors at the DWA level produces a non-linear Automation Index concentrated on a discrete five-point set, and identified *Cognitive Risk Asymmetry*, the systematic +0.35 inflation in expert-perceived risk relative to AI-rated risk in high-stakes regulatory domains, as the structural mechanism. That paper, however, could not specify what was happening beneath the DWA aggregate; it could only document that *something* non-continuous was operating. The present paper supplies the missing structural account: the bipolar action distribution is the deeper substrate that produces the non-linear DWA-level OAI shape observed in Gao et al. (2026) at higher aggregation levels. Read together with that prior work, the present paper completes a multi-level challenge to the Routine-Biased Technological Change paradigm (Autor et al., 2003): the routine/non-routine binary that grounded RBTC is too coarse to capture occupational substitutability under generative AI; the actual structure visible at the action level is a **bipolar structure** between physical-tool execution and cognitive planning, with a thick low-contrast middle that no single capability axis predicts. The implication for the empirical literature is concrete: indices that report “moderate” substitutability for an occupation are reporting the location of an occupation in this low-contrast middle, a region where the typology discriminates only weakly, rather than locating it on a smooth gradient.

The same observation applies to recent work that has begun documenting within-occupation heterogeneity (Henseke et al., 2025) or extending exposure to agentic AI capabilities (Gupta and Kumar, 2026). These contributions enrich the input variables but retain the linear-aggregation operator that produces the smooth-looking output. The structural diagnosis we offer is that the operator, not the input, is what hides the polarity: changing what one rates, while preserving how one aggregates the ratings, leaves the gradient appearance intact. The remedy is not to add more capability dimensions to the rating step but to change the aggregation rule, or, as in this paper, to refuse aggregation entirely and inspect the underlying distribution.

We apply the same critique to our own headline $K = 7$ partition. As shown in §4.4, M4 (Diagnostic Analysis) is itself a chimera that holds three semantically distinct sub-clusters (HVAC, patrol, data) under the umbrella of a shared surface lexicon (*inspect, examine, review*). The internal OAI range of M4 (0.573) is larger than the headline $K = 7$ M2-vs-M7 gap (0.45). Honest reporting requires us to say that the $K = 7$ partition is not unique; finer resolutions resolve more contrast, and the M4 cell is the specific place where this matters most. The bipolar

shape itself is invariant, but the labels we assigned to the poles, “M2” and “M7”, are properties of the $K = 7$ cut. At $K = 12$, M4-HVAC moves into the low pole and M4-data moves into the high pole. The structural finding is the persistence of two poles plus a low-contrast middle; the macro labels are an aid to interpretation, not the finding itself.

6.2 The RPA–AI Boundary: Insight from M3

The most informative single feature of the M3 (Iterative Repetition) macro is what it does *not* do: no DWA in the dataset has M3 as its dominant macro. Every DWA in which a C9 “repeat steps k to ℓ ” action appears has it as a minority step embedded within actions belonging to other macros. Structurally, this means that “repeat” is a sub-action across domains, not a domain in itself. The implication for the practical automation literature is direct: many treatments of occupational automation conflate two technically distinct frontiers that the M3 finding empirically distinguishes.

Robotic Process Automation (RPA), as reviewed by [Ivančić et al. \(2019\)](#), targets exactly the kind of structured repetitive sub-action that M3 captures: rule-based loops over data entry, file transfers, transaction reconciliation, and form processing. RPA tools succeed on these sub-actions precisely because the actions are repetitive and rule-bounded; they do not require domain-specific reasoning. Generative AI substitution, in contrast, targets the surrounding domain-specific reasoning embedded in M1, M2, M4, M5, M6, and M7: reading a chart, drafting a plan, advising a client, executing a tool-mediated physical task. The two technologies operate on orthogonal sub-structures within the same DWAs.

Past empirical work that produces a single substitutability score per occupation conflates these two automation frontiers. An occupation with many repetitive sub-actions and a thin layer of domain reasoning will receive a similar aggregate score to an occupation with few repetitive sub-actions and a thick layer of domain reasoning, even though the two are vulnerable to entirely different technologies on entirely different deployment timelines. Concretely, an accounts-payable clerk and a junior auditor may both score in the middle band of an aggregate substitutability index. The clerk’s exposure is dominated by M3-style repetitive transactions vulnerable to commodity RPA tooling that has been mature for nearly a decade; the auditor’s exposure is dominated by M4-style diagnostic and M5-style verification reasoning vulnerable to a generative-AI deployment frontier whose commercial robustness remains contested. Treating the two as comparable on a single index conflates a deployed technology with an emerging one. Our typology empirically demonstrates the distinction: M3 identifies the RPA-vulnerable sub-action layer, while the seven domain-thematic macros identify the AI-vulnerable layer. A serious occupational forecasting model needs both axes; treating the M3 sub-action mass and the domain-action mass as substitutable inputs to a single aggregate is the central methodological error our typology surfaces.

6.3 The Generic Substrate and Its Significance

The 35.6% noise group is not a clustering failure; it is a structural feature of occupational micro-action data. As shown in §4.6, the noise group’s distributions of `mapped_stage`, cognitive-physical orientation, sequential position, and OAI all reproduce the population shape to within

one to two percentage points; the Kolmogorov-Smirnov test on OAI returns $p = 0.851$. Roughly one-third of occupational micro-actions are domain-neutral generic verbs (*review, identify, document, ensure, relevant*) that span every occupation and every process stage without forming a coherent topical neighbourhood.

Three implications follow. First, models that predict substitutability from occupation-level or DWA-level features systematically miss this layer because the substrate is invisible at coarser aggregation: averaging substrate actions over a DWA leaves no distinguishing trace. Second, the substrate is plausibly exactly the layer at which contemporary LLMs already operate effectively (generic information processing, document summarization, status-update authoring, routine review tasks), but the gradient assumption made the substrate invisible by averaging it into surrounding domain-specific actions. Third, for task-based wage models in the [Acemoglu and Restrepo \(2022\)](#) tradition, the substrate suggests that 35% of the cost basis of many occupations is potentially LLM-substitutable in a way that cannot be read off a continuous task index. The task-based framework of [Acemoglu and Restrepo \(2018, 2022\)](#) decomposes aggregate labour demand into the contribution of automated tasks and non-automated tasks, and traces wage and employment outcomes to the balance between a displacement effect (automation removes tasks from workers) and a reinstatement effect (new tasks are created). When the substrate is treated as 35% of micro-action mass distributed across every occupation, the displacement-versus-reinstatement balance shifts in ways the task-level implementation cannot detect. In the standard implementation, displacement is modelled as a reallocation of task shares *across* occupations, with task-exposure scores aggregated to the occupation level before entering the wage equation. A substrate that is uniformly distributed across occupations contributes equally to every occupation’s aggregated task-exposure score, and therefore cannot drive cross-occupational wage differentials in this framework even if it is the layer most directly substituted. The implication is sharp. Within-occupation displacement of 35% of action mass, with no change in occupational headcounts, would generate wage compression of comparable magnitude on the same horizon as the displacement, but it would do so as a within-occupation effect invisible to cross-occupational regressions of wage on task-exposure score. The reinstatement effect, in turn, would have to operate at the within-occupation level (new substantive tasks created *within* each preserved occupational title to absorb the workers whose substrate hours were eliminated) rather than at the cross-occupational level. Disaggregation of substrate-versus-domain action mass is therefore necessary before existing OAI-style indices can be mapped onto wage- or employment-share predictions with reasonable confidence, and the substrate finding suggests that a refined task-based model would need to track substrate-share and domain-share separately and let them enter the wage equation with different coefficients.

A separate point of emphasis: the substrate’s invariance across four independent feature dimensions is a stronger empirical claim than any single-dimension test. Each dimension on its own admits an alternative explanation, since a single matched moment could plausibly arise from coincidence, but four independent dimensions converging to within one to two percentage points each rules out coincidence as a viable account. It is the convergence of four indistinguishability results, not any individual KS or proportion comparison, that licenses the structural reading. The substrate is, in this sense, the population shape itself viewed at action resolution: the actions

that are everywhere and nowhere in particular, doing the same proportional work across every occupation regardless of the occupation’s specific domain. The literature on AI substitution has been systematically blind to this layer because the layer becomes invisible the moment one aggregates to the DWA or occupation level, it is the only set of actions whose aggregation produces no signal worth reporting, and so it has been routinely averaged away.

The substrate as “white-collar dark matter” and its displacement form. Read through a management-theoretic lens, the 35.6% substrate is not a clustering artifact to be apologised for; it is the empirical manifestation of what organisation theorists since [Mintzberg \(1973\)](#) have called the *unrecorded layer of managerial and professional work*, the verbs (“ensure,” “document,” “review,” “follow up”) that no job description names but that consume roughly one-third of every white-collar workday. This layer is methodologically invisible to task-based exposure indices because it does not cluster into a topical neighbourhood; it is substantively invisible to occupational classification because it does not define any occupation. Yet it is *uniquely substitutable by current generative AI*. Producing a status update, drafting a follow-up email, summarising a meeting, formatting a quarterly review, and identifying relevant material from a document corpus are precisely the operations contemporary LLMs already perform competently at marginal cost. The displacement implication is asymmetric and, critically, of a qualitatively different form from the wave-forecast tradition’s predictions. Rather than wiping out occupations from the bottom up, generative AI may *compress the substrate within* every occupation, leaving formal job titles intact while extracting one-third of their actual time content. This is structurally a *flattening dynamic* (fewer hours of generic substrate work per occupation, with the domain-specific actions that survive becoming a larger share of each occupation’s residual content) rather than a *displacement dynamic* in which entire occupations move from employment to non-employment. Standard occupation-level exposure indices cannot detect this dynamic because the substrate is precisely the layer that aggregates away; they will report low exposure for occupations whose substrate share is being compressed even as employers internally reorganise around the smaller residual. The empirical prediction is sharp: white-collar wage pressure under generative AI will not manifest as the displacement projections in [Ellingrud et al. \(2023\)](#) predict (twelve million transitions across occupational categories), but as compression of within-occupation time use (fewer assistants per partner, fewer juniors per senior, fewer support roles per substantive role) with occupational labels largely preserved. Standard cross-sectional exposure indices, ours included, were not built to detect a within-occupation flattening; future work decomposing each occupation’s time budget into substrate versus domain-specific components is needed to test this prediction directly.

6.4 A Formal Account of Reversing Poles

The bipolar geometry and its decade-scale inversion can be given a compact formal representation that makes the “stable geometry, reversing poles” framing literal rather than metaphoric. Let an occupation j be represented as its composition over the four intelligence types of §3.6:

$$\omega_j = (\omega_{L,j}, \omega_{M,j}, \omega_{E,j}, \omega_{H,j}), \quad \sum_k \omega_{k,j} = 1, \quad (1)$$

where L denotes Linguistic, M Multimodal Perception, E Embodied, and H Human-Bound capacity. The vector ω_j is the action-level resource composition of occupation j , the empirical object we recover in this paper by clustering 15,817 micro-actions and aggregating to the $K=7$ macros. *It is durable: it is a property of how occupational work is structured at the action level, not of the technology available to substitute for it.*

The era-specific substitutability of occupation j in era t then takes the form of a linear projection of the stable composition ω_j onto two era-specific vectors:

$$S_j(t) = \sum_{k \in \{L, M, E, H\}} \omega_{k,j} \cdot \Psi_k(t) \cdot \Gamma_k(t), \quad (2)$$

where $\Psi_k(t) \in [0, 1]$ is the technical capability frontier of contemporary AI for intelligence type k at time t , and $\Gamma_k(t) \in [0, 1]$ is the era’s institutional, regulatory, and physical risk-tolerance multiplier for deploying that capability in commercial use. The two multipliers correspond in spirit to the technical-capability and compliance-risk factors independently identified in [Gao et al. \(2026\)](#): Ψ is the technological capability factor, Γ is the inverse of the compliance-and-risk factor whose Cognitive Risk Asymmetry mechanism was documented at the DWA level. Equation (2) states the substantive content of this paper compactly: **action-level substitutability is the product of (i) a durable resource composition, (ii) an era-contingent technical capability frontier, and (iii) an era-contingent institutional risk tolerance.**

The 2013 and 2026 capability frontiers. The decade-scale polarity inversion documented in §5 is, in this notation, a radical rotation of $\Psi(t)$ between two anchor years. In 2013 the engineering-bottleneck consensus underlying [Frey and Osborne \(2017\)](#) positioned the capability frontier at structured physical execution and routine symbolic manipulation, with natural-language understanding and unstructured planning identified as the durable bottlenecks. In 2026, after the deployment of large-scale Transformer-based foundation models, the frontier has rotated almost orthogonally: general-purpose language processing and multi-step symbolic reasoning have crossed the bottleneck threshold, while general physical manipulation in unstructured environments remains constrained by hardware and embodiment limitations. Concretely, we can summarise the two frontiers as

$$\Psi(t_1=2013) \approx (0.10, 0.30, 0.80, 0.05), \quad \Psi(t_2=2026) \approx (0.95, 0.70, 0.15, 0.20), \quad (3)$$

where the four components are $(\Psi_L, \Psi_M, \Psi_E, \Psi_H)$. The numerical values in (3) are illustrative rather than fitted, the model is identified only up to monotone transformations of Ψ , but the qualitative claim is sharp and falsifiable: between t_1 and t_2 , Ψ_L and Ψ_E have approximately exchanged ranks.

The closed-form polarity inversion. Substituting (3) into (2) and taking the era-to-era difference gives the substantive content of the polarity inversion:

$$\Delta S_j = S_j(t_2) - S_j(t_1) \propto \omega_{L,j} - \omega_{E,j} + (\text{smaller terms in } \omega_M, \omega_H). \quad (4)$$

The poles of the bipolar structure are therefore not arbitrary macros but the macros whose ω_j is most concentrated on a single intelligence type. Reading from Table 5 (intelligence-type composition by macro), M7 (Planning & Design) has $\omega_L = 0.95$ and $\omega_E = 0.03$, so $\omega_{L,j} - \omega_{E,j} = 0.92$, among the largest positive values in the typology, predicting the largest era-to-era rise in S_j . M2 (Tool-Mediated Physical Execution) has $\omega_L = 0.15$ and $\omega_E = 0.56$, so $\omega_{L,j} - \omega_{E,j} = -0.41$, the largest negative value, predicting the largest era-to-era fall in S_j . The empirically observed reversal in Table 7 (M7’s mean exposure rising from 0.287 under Frey-Osborne to 0.504 under OAI; M2’s mean falling from 0.703 to 0.058) is precisely the qualitative pattern that (4) predicts. The macro-level Spearman $\rho = -0.750$ between Frey-Osborne and Eloundou rankings (§5.2, Table 8) is, in this notation, the rank-correlation analogue of the sign change in $\omega_{L,j} - \omega_{E,j}$ being projected onto a rotated Ψ .

Stable geometry, reversing poles, formalised. Equation (2) makes the title metaphor literal. The *stable geometry* of our title is the matrix of action compositions $\{\omega_j\}$, durable across capability eras because it is a property of how human work is structured rather than of which technologies can substitute for it. The *reversing poles* of our title are the shifting components of $\Psi(t)$, which determine, era by era, which fixed ω_j projection sits at the high pole and which at the low. The bipolar shape is the durable property of $\{\omega_j\}$: there exist occupations near every extreme of $\omega_{L,j} - \omega_{E,j}$, so any $\Psi(t)$ that maps differently across L and E produces two poles plus a middle band. The polarity of the bipolar shape, which extreme of $\omega_{L,j} - \omega_{E,j}$ is the high pole, is the era-contingent property of $\Psi(t)$. A future capability era in which embodied AI matures decisively, raising Ψ_E relative to Ψ_L , would produce another rotation of the polar identities while leaving the bipolar shape itself intact; (2) predicts such a rotation directly. The robustness checks reported throughout §4.3 address the durability of ω_j ; the temporal-axis result of §5 addresses the contingency of $\Psi(t)$. Together they characterise the structural object that the present paper introduces and that future labour-substitution research can transport across capability eras: the matrix $\{\omega_j\}$ of action-level resource compositions, paired with a forecastable $\Psi(t)$ trajectory.

6.5 Responding to the 2026 Wave: Why the Stable Geometry Matters

The capability-stage frameworks and wave-of-displacement forecasts surveyed in §2.4 share a structural reliance on the contemporaneous capability frontier as the anchor for projection. The pattern is familiar: estimate today’s capability, extrapolate forward, read off an exposure score per occupation, sort occupations by score, declare a wave. This pattern has been instantiated in academic capability-level papers (Morris et al., 2024), industry stage announcements (Metz, 2024), and the most widely-cited consulting projections (Chui et al., 2023; Ellingrud et al., 2023). The empirical result we report in §5 interrogates this pattern directly.

The **polarity inversion** between 2013 and 2026 (with the macros at the high-FO pole now sitting at the low-OAI pole and vice versa, at macro-level Spearman $\rho = -0.750$ against the Eloundou 2023 indicator) establishes that the wave-forecast pattern has already failed once at a thirteen-year horizon. The 2013 Frey-Osborne reading of which occupations were most exposed to automation, projected forward, gave a pattern in which Tool-Mediated Physical

work was most at risk and Planning & Design was safest. This was a reasonable forecast from the engineering-bottleneck literature [Frey and Osborne \(2017\)](#) drew on, which emphasised the unsolved problems in robotics, manipulation, and unstructured perception. The forecast was structurally wrong about polarity content because the dominant AI-capability frontier of the subsequent decade turned out to be Linguistic and Multimodal Perception, not Embodied. The macros aligned with the Linguistic intelligence type (M7 Planning & Design, M4-data, and M5) rose to the high-OAI pole; the macros aligned with Embodied and Multimodal Perception (M2, M4-HVAC, and M4-patrol) fell to the low-OAI pole.

The substantive lesson is not that the 2013 forecast was poorly made. It is that any single-point exposure forecast inherits the era’s dominant capability axis and reverses when the axis moves. The polar reversal is the existence proof: it has happened once. The wave forecasts assembled for the present moment, [Chui et al. \(2023\)](#) and [Ellingrud et al. \(2023\)](#) both anchor on a 2023-vintage generative-AI capability projection, inherit the assumption that the Linguistic-frontier axis will remain dominant for the next decade. They may be right; they may be wrong; but the empirical question of which is which cannot be answered from inside the contemporaneous capability frame. What can be transported across capability eras, and what we therefore propose as the robust object of empirical interest, is the **stable geometry**: the existence of two poles plus a low-contrast middle band, the bipolar shape itself, and the intelligence-type mechanism that determines which type maps to the high-exposure pole. These structural properties survive the indicator vintage check; the per-macro exposure rank does not.

The constructive recommendation is twofold. First, distinguish geometry from content in any forecasting exercise: the bipolar shape itself is a structural prediction (we expect two poles plus a middle, regardless of indicator era); the polar identity is a contingent prediction (which macros are at which pole depends on the dominant capability axis). Second, reverse the inferential direction. Rather than projecting an exposure score per occupation and inferring which occupations are at risk, infer which intelligence type the era’s dominant capability frontier targets, then look up which macros are aligned with that type. The substantive question becomes “which capabilities does the era unlock” rather than “which occupations are exposed”. The latter follows mechanically from the former; the former is the genuinely uncertain quantity that the wave-forecast literature attempts to project without acknowledging the contingency.

6.6 Methodological Implications

Beyond the substantive findings, the pipeline we present has methodological transferability. We highlight five practices that other researchers may adopt.

Multi-layer clustering. Combining HDBSCAN at fine granularity with hierarchical Ward linkage at coarse granularity recovers structure at multiple natural resolutions, where neither method alone would suffice. HDBSCAN’s variable-density advantage handles local heterogeneity (no requirement that clusters be spherical or equally-sized), while Ward linkage on engineered cluster-level features produces an interpretable macro typology amenable to substantive labeling. Occupational data is multi-resolution by construction, occupations contain DWAs contain micro-actions; the lexical structure visible at the action level is different in kind from the workflow structure visible at the DWA level, and clustering at a single resolution discards structure at the

others.

Distributional shape testing. The Hartigan dip test and the two-sample Kolmogorov-Smirnov test are routine in non-parametric statistics but rare in empirical AI-exposure research. We argue they should be standard. Most prior work skips the question of distributional shape and proceeds directly to aggregate moments, implicitly assuming unimodality and continuity. The dip test on M2’s OAI distribution rejected unimodality at the 1% level, an empirical fact that no aggregate-moment summary would have surfaced. Distributional testing is cheap, well-understood, and prevents the analyst from conflating “high variance” with “high mean uncertainty” when in fact the variance is structured by hidden modes.

Cross-aggregation external validity. Projecting the OAI from Gao et al. (2026) onto the present paper’s typology is a transferable validation pattern: when two methodologically independent procedures (Tech-Risk-DWA aggregation in the prior work versus action-level semantic clustering in the present paper) converge on the same partition of occupational substitutability, each procedure validates the other. We recommend cross-aggregation projection as a routine external-validity check for clustering-based labour-market typologies. The cross-indicator reproduction shown in §4.7, Eloundou, AIOE, and FO all reproducing the bipolar shape, is an instance of the same pattern at a different level: when three indicators computed by three entirely different procedures all yield two poles plus a middle band on the same macro typology, the typology has captured something more than any single indicator’s bias.

Honest treatment of unclustered data. Rather than forcing the 35.6% noise points into nearest clusters, we preserved them as a distinct analytical group and characterised their distributional invariance separately. The choice surfaced the generic-substrate finding (§6.3). Forcing-to-nearest would have absorbed the substrate into the seven domain macros and hidden a substantively important structural feature behind a clean-looking taxonomy. The default disposition in much applied clustering work is to treat HDBSCAN’s noise label as an implementation defect to be smoothed away; we recommend the opposite disposition, especially in social-science domains where the noise label may carry structural information about the domain itself rather than about the algorithm.

Encoder-supervised triangulation. For supervised classification steps embedded in unsupervised pipelines, e.g., the four-way intelligence-type assignment in §3.6, the standard practice of picking a single encoder is brittle. We recommend running the classification under two independent encoder families and ratifying the labels against a stratified human audit. In our application, the MPNet \leftrightarrow BGE Cohen’s κ of 0.666 across the full dataset is moderate (and would be the only available robustness check absent the audit), but the 150-row human audit reveals an asymmetric story: BGE matches the human at $\kappa = 0.893$ versus MPNet’s $\kappa = 0.769$, with the gap concentrating on the 30 rows where encoders disagreed. This combination of (a) encoder triangulation and (b) human audit is what licensed the encoder switch from MPNet (used for clustering) to BGE (used for intelligence-type classification). Either check alone would have been weaker.

6.7 Theoretical Contributions to Organisation Theory

The substantive contributions of this paper to organisation theory are distinct from its methodological and empirical contributions, and merit a separate articulation. Three propositions follow from the analysis above; each engages a long-standing position in the management-theoretic literature.

Proposition 1: The analytical unit of labour-substitution theory is the action, not the occupation or the task. (*Formally:* the matrix $\{\omega_j\}$ of §6.4 is the empirically tractable object; aggregations to the task or occupation level discard the dimensional structure that the bipolar geometry exposes.) This is a microfoundational claim in the sense of Felin et al. (2012). The bipolar geometry we document at the action level disappears at the DWA level and is invisible at the occupation level; methodological commitment to a coarser unit *constructs* the smooth-substitutability appearance that exposure indices then “discover.” The continuous-gradient tradition (§2.1) is not measuring a property of work; it is measuring an artifact of its own aggregation rule. The implication is that the standard analytical scaffolding of the AI-substitutability literature, ability-weighted exposure scores, task-level exposure tiers projected to occupations, capability-stage forecasts read off occupational distributions, is structurally incomplete. Recovering the underlying substrate requires going below the task, which the microfoundations programme has been arguing organisation theory must do for two decades and which the labour-economics literature has not yet operationalised at the action layer.

Proposition 2: Capability heterogeneity is the durable structure; valuation is the era-contingent overlay. (*Formally:* ω_j is invariant across t ; $\Psi(t)$ varies; see equations (1)–(4).) This extends the resource-based view (Penrose, 1959; Barney, 1991; Grant, 1996) along a dimension that the original formulation did not need to address: time. Read through Barney, the four intelligence types (Linguistic, Multimodal Perception, Embodied, and Human-Bound) are the durable resources whose composition varies across occupations and confers competitive insulation against substitution. Read through the polarity inversion (§5), which resource type confers insulation in a given era is itself a function of which capability frontier the era’s dominant general-purpose technology has crossed. The 2013 Frey-Osborne reading placed Embodied capacity at the high-OAI pole because robotics was the era’s frontier expectation; the 2026 LLM reading places Linguistic capacity at the high-OAI pole because language modelling has been the era’s actual frontier. The capability-trajectory mechanism is concrete: early-2010s automation projections extrapolated from rule-based and robotic-process tooling whose strength lay in structured, deterministic sub-tasks, whereas the 2020s capability frontier has been driven by foundation models whose generalisation across unstructured language and pattern-recognition tasks crossed the bottlenecks the Frey-Osborne dimensions had assumed durable. The resource is durable. The labelling of which resource confers “rare, valuable, inimitable, non-substitutable” protection is not. This is a non-trivial qualification of the resource-based view’s temporal stability assumption and applies symmetrically to any general-purpose technology whose capability frontier shifts across the strategic-planning horizon of firms holding heterogeneous resource portfolios.

Proposition 3: Generative AI’s distinctive substitution risk lies in the substrate it compresses, not in the occupations it disrupts. (*Formally:* the noise group, statistically indistinguishable from the population across four feature axes, behaves as a fifth invariant entry in ω_j that is shared by every occupation; current Ψ_L acts directly on it.) This is a routine-dynamics implication in the sense of [Pentland and Feldman \(2005\)](#): the 35.6% generic-action substrate is the ostensive layer common to every occupational routine, executed everywhere, recognised nowhere as the substantive content of any specific occupation, and now maximally exposed to current LLM capability. The displacement form predicted by our analysis is therefore organisational flattening within preserved occupational titles, not occupational extinction. This proposition stands in direct tension with the wave-forecast tradition (§6.5), which models displacement as cross-occupational reallocation; it stands in agreement with the operational realities reported by enterprises adopting generative AI, which document compression of support layers rather than reassignment of substantive roles. The empirical test that would distinguish the two forecasting frames, per-occupation longitudinal time-budget tracking of substrate-versus-domain action shares, is not currently available at scale, but the present analysis suggests it is the next datum the field should be collecting.

Proposition 4: Exposure is not displacement: the bipolar structure carries an asymmetric substitution-vs-augmentation prediction across its poles. (*Formally:* the $\Gamma_k(t)$ multiplier in equation (2) captures the regime-dependent translation of action-level exposure into either substitution or augmentation; substitution-vs-augmentation is the empirical content of Γ , not of Ψ .) The OAI we project measures task-level exposure, not job-level displacement; the substitution-vs-augmentation distinction articulated by [Acemoglu and Restrepo \(2018, 2022\)](#) is therefore not a peripheral caveat but a structural reading of the bipolar shape. The two poles and the middle band map onto qualitatively different deployment regimes. **The high-OAI pole (M7 Planning & Design, M4-data, M5)** is the region where current LLM capability is most plausibly *augmentative*: the constituent actions, drafting specifications, verifying data accuracy, producing stakeholder reports, are precisely the operations where Copilot-style integration raises per-worker output without removing the need for the worker, because residual judgement, accountability, and integration with downstream organisational decisions remain human responsibilities. We therefore expect the high-OAI pole to manifest empirically as productivity expansion within preserved occupational headcounts rather than as headcount contraction, at least in the short to medium term. **The low-OAI pole (M2 Tool-Mediated Physical, M4-HVAC, M4-patrol)** is structurally protected from both regimes: neither substituted by current LLMs (the actions require embodied execution that contemporary AI cannot perform) nor augmented by them (the productivity gain from adding language-model support to a roofer or HVAC technician is bounded by the irreducible physical content of the work). **The middle band, and especially the 35.6% generic-action substrate**, is where direct substitution is most concentrated. The substrate consists of generic verbs, ensure, document, review, follow up, that AI can perform end-to-end with marginal human oversight; this is exactly the layer that compresses (§6.3) rather than augments. The asymmetry is sharp: the bipolar structure predicts *augmentation at the high pole, no change at the low pole, and*

substitution-via-compression in the middle and the substrate. Existing single-scalar exposure indices cannot distinguish these regimes because they treat exposure as a one-dimensional risk; treating the bipolar structure as primary and asking, per macro, what the residual human contribution looks like, is the analytical move that lets the substitution-augmentation distinction become tractable rather than rhetorical.

Together these four propositions reframe the contribution of the paper. The bipolar geometry is not just a statistical finding about an OAI distribution; it is evidence for a microfoundational repositioning of the labour-substitution-theoretic unit of analysis, an extension of resource-based theorising to temporally non-stationary capability frontiers, a routine-dynamics-grounded prediction about the form generative-AI displacement will take, and a structural mapping between the bipolar geometry and the substitution-vs-augmentation distinction that contemporary task-based automation theory has placed at the centre of its empirical agenda.

6.8 Limitations

Eight limitations qualify the contribution. We list them honestly so that subsequent work can target them directly.

LLM-generated micro-actions may carry model-specific bias. The 15,817 micro-actions were generated by a multi-agent LLM pipeline calibrated against the variance-driven HITL panel of Gao et al. (2026). Cross-model voting and HITL anchoring mitigate single-model bias substantially, but they do not eliminate the possibility of systematic distortions shared across LLMs trained on overlapping web corpora. The bipolar finding is robust insofar as it survives the cross-aggregation external validity check against the independently calibrated DWA-level OAI of Gao et al. (2026) and reproduces under Eloundou et al. (2024) GPT-4 task labels; however, replication with non-LLM action decomposition (expert-only, or worker-survey-derived) remains a future-work item.

English-only, US-based occupational ontology, and the Global South question. O*NET is a US labor-market ontology curated in English, and the analysis we report is therefore best read as a structural diagnosis of the US economy under US occupational categories. Three specific generalisability concerns follow from this scope. First, O*NET’s occupational coverage reflects the sectoral composition of a high-income post-industrial economy: services dominate, manufacturing is comparatively compressed, and agricultural and informal-sector work are heavily under-represented. Economies with a larger manufacturing share (most middle-income economies in East and Southeast Asia, and large parts of Latin America) may show a different macro-level distribution of micro-actions, with a heavier weighting on M2 (Tool-Mediated Physical Execution) and M4-HVAC (physical equipment monitoring) at the population level. Second, O*NET’s classification logic presupposes a formal labour market in which occupations are defined, named, and described against a stable institutional template; economies with substantial informal employment (in which workers move flexibly across multiple income-generating activities without occupying a single formal occupation) cannot be straightforwardly mapped onto the DWA framework at all. The bipolar structure we document may therefore be partially an artifact of the formalised occupational ontology rather than a property of generative-AI substitutability per se. Third, our semantic encoder is trained predominantly on English-language corpora, and the

four-way intelligence-type classification was validated against an English-language human audit. Cross-language replication, particularly in non-Indo-European languages where occupational vocabulary and the cognitive-physical action distinction may be lexicalised differently, is required before the bipolar shape and the polarity-inversion finding can be claimed as features of generative-AI substitutability in general rather than of generative-AI substitutability in the US-formal-economy subset. Future cross-country work using harmonised occupational ontologies (ILO ISCO-08, OECD PIAAC skill measurement, the EU ESCO taxonomy) and multilingual encoder validation is the natural next step; until that work is done, the geographic and linguistic scope of our claims should be read as US-formal-economy rather than as universal.

The temporal-axis claim rests on $n = 9$ macros. The Spearman correlations underpinning the polar reversal (§5.2) are computed across nine macros: $n = 9$ is a small sample for a rank-correlation test, and the FO \leftrightarrow OAI p -value of 0.058 sits at the edge of conventional significance. The FO \leftrightarrow Eloundou p -value of 0.020 is comfortably significant. The qualitative claim, that the polar identities swap between FO and the LLM-era indicators, is robust to this n via the per-macro rank movements (§5.2, last paragraph), but a formal trend analysis at finer granularity than nine macros would require either a finer macro partition or a non-rank test.

The era-gradient observation rests on $n = 4$ indicators. The monotone increase in middle-pair non-significance from 33% (FO 2013) to 100% (OAI 2026) is striking but supported by only four indicators. We report it descriptively only and refrain from a formal trend test; the substantive temporal claim is the polar reversal, not the era-gradient observation.

OAI inherited from Paper 1. All limitations of Gao et al. (2026), including the LLM-rater bias on Tech and Risk scoring, the panel composition of the 31-expert HITL validation, and the heuristic 0.3, 0.5, and 0.7 discrete adoption thresholds, propagate into the present paper through the projection. The bipolar finding survives because its dependence on OAI is structural rather than parametric; small recalibrations of the OAI matrix would not flip M2 and M7’s relative positions, but they would shift mean values within the middle band.

Encoder dependence partially mitigated, not eliminated. For the intelligence-type classification we switched from MPNet to BGE on the basis of the 150-row human audit (§3.6). The audit is necessary evidence, but it is not exhaustive: 150 rows out of 15,817 is a stratified probe, not a complete labelling. A larger human audit (1,000+ rows) would be useful, particularly for the M4 chimera region and the ambiguous boundary between Linguistic and Multimodal Perception. The encoder-pair check would also benefit from a third encoder family such as E5 or GTE, but the practical resource constraints in our environment did not permit this.

The four-way intelligence-type decomposition is an interpretive lens, not a uniquely correct taxonomy. As stated in §3.6, the Linguistic, Multimodal Perception, Embodied, and Human-Bound classification we use is one defensible decomposition of contemporary AI capability, not a new taxonomic theory proposed by this paper. Alternative published decompositions partition the same underlying space differently: Morris et al. (2024) use a six-level performance ladder; the OECD AI Capability Indicators use nine ability domains crossed with five capability levels; Metz (2024) use five sequential stages. Our four-way scheme was chosen because it maps cleanly onto the four primary technical bottlenecks contemporary AI systems face, because the 150-row human audit validates it at $\kappa = 0.893$ for our specific use case, and

because the four-way granularity is interpretable without becoming unwieldy. None of these reasons privileges the four-way choice as uniquely correct. Future work using finer or differently-cut intelligence-type taxonomies (Morris-level capability gradations, OECD-domain \times level cells, or a yet-finer decomposition derived from data) could legitimately reach different mechanistic readings of the same OAI distribution. The mechanism reading we report in §4.8 (Linguistic-class OAI lead of $3.37\times$) is sufficient to support the bipolar-structure-with-polarity-inversion findings of the present paper, but it is not the only such reading consistent with the data, and we do not claim otherwise.

$K = 7$ may still be too coarse. The intra-cluster bifurcation observed within M2 (§4.5) and the M4 chimera (§4.4) both indicate that finer hierarchical layers are warranted. The resolution sweep through $K = 15$ documents this directly: the polar gap widens at finer resolutions, and middle-pair non-significance drops. A future paper could explore $K = 10$ to $K = 15$ with stronger bifurcation testing, possibly producing a three-level taxonomy (macro / meso / micro) rather than the two-level structure we report here. The same logic likely applies to the more cognitive macros (M5, M6, M7), where the within-macro semantic content is internally diverse on dimensions our 15-d feature vector did not capture; a richer feature set incorporating tool-use, regulatory environment, or stakeholder count could surface additional structure beneath what we currently report as homogeneous middle-band macros.

Static cross-section. The analysis is a single-time-point snapshot. The polarity-inversion claim is constructed by comparing two single-time-point indicators (FO 2013 and OAI 2026); we do not have year-by-year longitudinal data tracing the inversion’s trajectory. A longitudinal repetition over the next three to five years would convert the inversion claim into a developmental claim and would permit observation of whether the geometry itself begins to widen, narrow, or fragment under continued capability advance.

7 Conclusion

We decomposed 1,961 O*NET Detailed Work Activities into 15,817 micro-actions and applied a two-stage clustering pipeline, with HDBSCAN at the micro-cluster level and hierarchical Ward linkage at the macro level, to produce seven domain-thematic macros, one singleton meta-action layer (M3, Iterative Repetition), and a 35.6% generic-action substrate. Projecting the DWA-level Occupational Automation Index of Gao et al. (2026) onto this typology yielded two findings that together characterise the structural object the present paper introduces.

The spatial-axis finding is the **bipolar structure**: Tool-Mediated Physical Execution (M2, mean OAI 0.054) and Planning & Design (M7, mean OAI 0.499) form two extremes separated by Cohen’s $d = 2.41$, with six middle macros occupying a low-contrast band between them. This geometry is robust to three independent stress tests: clustering resolution (the polar gap widens from 0.45 at $K = 7$ to 0.57 at $K = 12$), encoder family (MPNet and BGE both reproduce the LLM-class OAI lead within $0.2\times$), and indicator choice (Eloundou’s GPT-4 task ratings, Felten’s AIOE, and Frey-Osborne’s computerisation probability all reproduce the bipolar shape). The middle is a low-contrast band, not absent contrast: two-one-sided tests at $d = 0.2$ admit only 1/15 pairs as equivalent. The M4 macro is itself a chimera that holds a 0.573-wide OAI range

under a single lexical umbrella; the headline $K = 7$ partition is privileged not as unique but as the coarsest cut at which the bipolar shape and the domain semantic labels are both legible.

The temporal-axis finding is the **polarity inversion**: the same macros under Frey-Osborne’s 2013 computerisation probability take a polar ordering that is the exact inverse of their LLM-era OAI ordering (macro-level Spearman $\rho = -0.750$ against Eloundou’s 2023 task labels, $p = 0.020$, computed against the original Oxford Martin appendix data). The macros aligned with the Linguistic intelligence type rose to the high-OAI pole; those aligned with Embodied and Multimodal Perception fell to the low-OAI pole. The four-way intelligence-type classification (Kruskal-Wallis $H = 527.6$, LLM-class mean OAI 0.427 versus other-class mean 0.127, a $3.37\times$ ratio) supplies the mechanism: the era’s dominant capability axis determines which intelligence type sits at the high-OAI pole, and so a single-point exposure forecast inherits the era’s capability frontier and reverses with it.

The theoretical takeaway is double. First, the continuous-gradient assumption that has organised AI-substitutability research since Frey and Osborne (2017) is an aggregation artifact: linear summation of capability dimensions produces smooth-looking output even when the underlying micro-action substrate is bipolar with a low-contrast middle. When we refuse the aggregation step and inspect the substrate directly, the actual spatial structure of occupational AI-substitutability is bipolar, with two extremes plus a low-contrast middle rather than a continuum. Second, the structural object that is stable across capability eras is the **stable geometry** itself, namely the count of poles (two), the existence of a low-contrast middle band, and the intelligence-type mechanism that determines polar identity, not the per-macro exposure rank. Wave-of-displacement forecasts that read off occupation-level exposure projections from a contemporaneous capability snapshot inherit the era’s frontier and reverse with it; the bipolar geometry does not.

The substantive theoretical contribution, developed in §6.7, is to relocate the analytical unit of labour-substitution theory from the occupation to the action, and from the action’s surface description to the capability frontier its execution requires. Once relocated, the smooth-substitutability appearance that has organised AI-exposure research since Frey and Osborne (2017) is revealed as an artifact of aggregation, the resource-based view’s account of competitive insulation extends naturally to the era-contingent valuation of micro-action resources (Barney, 1991; Penrose, 1959), and the routine-dynamics tradition’s emphasis on the granularity of organisational action (Pentland and Feldman, 2005; Feldman and Pentland, 2003) acquires an empirical instantiation at the labour-market scale. The formal account of §6.4 consolidates these readings into a single algebraic statement: action-level substitutability is the linear projection of a stable resource composition ω_j onto an era-contingent capability frontier $\Psi(t)$ and an era-contingent risk-tolerance multiplier $\Gamma(t)$, with the bipolar geometry living in ω and the polarity living in Ψ . These are not auxiliary corrections to the wave-forecast programme; they are claims that the programme has been answering the wrong question. It projects which occupations will be exposed under tomorrow’s capability, when the empirically tractable question is which actions are exposed under today’s, and which substrate is being compressed in every occupation simultaneously. The enduring object of empirical interest is not the fluid exposure score assigned to an occupation today, but the durable architectural structure of the actions

that compose it.

Four lines of future work follow naturally. First, the typology generated here is the natural input to occupational mobility prediction: cosine similarity over the macro-share vector for each occupation provides a similarity metric that respects the polarity structure rather than averaging across it; we develop this idea in a separate paper currently in preparation. Second, cross-country and cross-language replication is needed to determine whether the bipolar shape is a feature of the US occupational ontology or a deeper structural property of generative-AI substitutability. Third, finer-grained typology testing at $K = 10$ to $K = 15$ would establish a three-level taxonomy (macro / meso / micro) and resolve the M4 chimera into its three substantively distinct sub-clusters. Fourth, the polarity-inversion finding invites a forward extrapolation that combines the bipolar geometry (transportable across eras) with explicit capability-frontier scenarios (the variable that determines polar identity), producing era-conditional exposure forecasts whose uncertainty is properly bounded by the structural variation we documented. A finer-resolution comparison of the present paper’s action-level typology against the capability-stage frameworks surveyed in §2.4 is the natural next step.

References

- Daron Acemoglu and Pascual Restrepo. The Race between Man and Machine: Implications of Technology for Growth, Factor Shares, and Employment. *American Economic Review*, 108(6): 1488–1542, 2018.
- Daron Acemoglu and Pascual Restrepo. Tasks, Automation, and the Rise in U.S. Wage Inequality. *Econometrica*, 90(5):1973–2016, 2022.
- David H. Autor, Frank Levy, and Richard J. Murnane. The Skill Content of Recent Technological Change: An Empirical Exploration. *The Quarterly Journal of Economics*, 118(4):1279–1333, 2003.
- Jay Barney. Firm resources and sustained competitive advantage. *Journal of Management*, 17(1):99–120, 1991.
- Ricardo J. G. B. Campello, Davoud Moulavi, and Jörg Sander. Density-Based Clustering Based on Hierarchical Density Estimates. In *Pacific-Asia Conference on Knowledge Discovery and Data Mining (PAKDD)*, pages 160–172, Berlin, Heidelberg, 2013. Springer.
- Michael Chui, Eric Hazan, Roger Roberts, Alex Singla, Kate Smaje, Alex Sukharevsky, Lareina Yee, and Rodney Zimmel. The Economic Potential of Generative AI: The Next Productivity Frontier. Report, McKinsey Global Institute, June 2023.
- James S. Coleman. *Foundations of Social Theory*. Harvard University Press, Cambridge, MA, 1990.
- David J. Deming and Kadeem Noray. Earnings Dynamics, Changing Job Skills, and STEM Careers. *The Quarterly Journal of Economics*, 135(4):1965–2005, 2020.

- Kweilin Ellingrud, Saurabh Sanghvi, Gurneet Singh Dandona, Anu Madgavkar, Michael Chui, Olivia White, and Paige Hasebe. Generative AI and the Future of Work in America. Report, McKinsey Global Institute, July 2023.
- Tyna Eloundou, Sam Manning, Pamela Mishkin, and Daniel Rock. GPTs are GPTs: Labor market impact potential of LLMs. *Science*, 384(6702):1306–1308, jun 2024. DOI 10.1126/science.adj0998. Data files used in this paper are taken from the 2023 working-paper release (arXiv:2303.10130); references to “Eloundou et al. 2023” in the body text refer to the vintage of the underlying GPT-4 task ratings rather than to the publication year.
- Martha S. Feldman and Brian T. Pentland. Reconceptualizing organizational routines as a source of flexibility and change. *Administrative Science Quarterly*, 48(1):94–118, 2003.
- Teppo Felin and Nicolai J. Foss. Strategic organization: A field in search of micro-foundations. *Strategic Organization*, 3(4):441–455, 2005.
- Teppo Felin, Nicolai J. Foss, Koen H. Heimeriks, and Tammy L. Madsen. Microfoundations of routines and capabilities: Individuals, processes, and structure. *Journal of Management Studies*, 49(8):1351–1374, 2012.
- Teppo Felin, Nicolai J. Foss, and Robert E. Ployhart. The microfoundations movement in strategy and organization theory. *Academy of Management Annals*, 9(1):575–632, 2015.
- Edward W. Felten, Manav Raj, and Robert Seamans. Occupational, Industry, and Geographic Exposure to Artificial Intelligence: A Novel Dataset and Its Potential Uses. *Strategic Management Journal*, 42(12):2195–2217, 2021.
- Carl Benedikt Frey and Michael A. Osborne. The Future of Employment: How Susceptible Are Jobs to Computerisation? Working paper, Oxford Martin School, University of Oxford, 2013. Working-paper antecedent of [Frey and Osborne \(2017\)](#). Cited here for the 702-row appendix table parsed programmatically in this paper’s external-indicator alignment; the published 2017 version contains the identical probability values (verified at Spearman $\rho = 1.000$ across 653 matched SOCs).
- Carl Benedikt Frey and Michael A. Osborne. The Future of Employment: How Susceptible Are Jobs to Computerisation? *Technological Forecasting and Social Change*, 114:254–280, 2017.
- Shuyao Gao, Minghao Huang, et al. Bounded by Risk, Not Capability: Quantifying AI Occupational Substitution Rates via a Tech-Risk Dual-Factor Model. *arXiv preprint*, 2026. arXiv:2604.04464.
- Paweł Gmyrek, Janine Berg, and David Bescond. Generative AI and Jobs: A Global Analysis of Potential Effects on Job Quantity and Quality. ILO Working Paper 96, International Labour Organization, 2023.
- Robert M. Grant. Toward a knowledge-based theory of the firm. *Strategic Management Journal*, 17(S2):109–122, 1996.

- Ravish Gupta and Saket Kumar. Agentic AI and Occupational Displacement: A Multi-Regional Task Exposure Analysis of Emerging Labor Market Disruption. *arXiv preprint*, 2026. arXiv:2604.00186.
- J. A. Hartigan and P. M. Hartigan. The Dip Test of Unimodality. *The Annals of Statistics*, 13(1):70–84, 1985.
- Golo Henseke, Rhys Davies, Alan Felstead, Duncan Gallie, Francis Green, and Ying Zhou. How Exposed Are UK Jobs to Generative AI? Developing and Applying a Novel Task-Based Index. *arXiv preprint*, 2025. arXiv:2507.22748.
- Lucija Ivančić, Dalia Suša Vugec, and Vesna Bosilj Vukšić. Robotic Process Automation: Systematic Literature Review. In Claudio Di Ciccio et al., editors, *Business Process Management: Blockchain and Central and Eastern Europe Forum (BPM 2019)*, volume 361 of *Lecture Notes in Business Information Processing*, pages 280–295. Springer, Cham, 2019. DOI 10.1007/978-3-030-30429-4_19.
- Leland McInnes, John Healy, and James Melville. UMAP: Uniform Manifold Approximation and Projection for Dimension Reduction. *arXiv preprint*, 2018. arXiv:1802.03426.
- Rachel Metz. OpenAI Sets Levels to Track Progress Toward Superintelligent AI. Bloomberg News, jul 2024. Industry framework; non-peer-reviewed. Reports OpenAI’s five-stage internal classification: Chatbots, Reasoners, Agents, Innovators, Organizations. URL: <https://www.bloomberg.com/news/articles/2024-07-11/openai-sets-levels-to-track-progress-toward-superintelligent-ai>.
- Henry Mintzberg. *The Nature of Managerial Work*. Harper & Row, New York, 1973.
- Meredith Ringel Morris, Jascha Sohl-Dickstein, Noah Fiedel, Tris Warkentin, Allan Dafoe, Aleksandra Faust, Clement Farabet, and Shane Legg. Position: Levels of AGI for Operationalizing Progress on the Path to AGI. In *Proceedings of the 41st International Conference on Machine Learning (ICML)*, volume 235 of *Proceedings of Machine Learning Research*, pages 36308–36321. PMLR, 2024. arXiv:2311.02462 (preprint Nov. 2023).
- Fionn Murtagh and Pierre Legendre. Ward’s Hierarchical Agglomerative Clustering Method: Which Algorithms Implement Ward’s Criterion? *Journal of Classification*, 31(3):274–295, 2014.
- OECD. Introducing the OECD AI Capability Indicators. Beta report, OECD Publishing, June 2025. Nine ability domains × five capability levels. URL: https://www.oecd.org/en/publications/2025/06/introducing-the-oecd-ai-capability-indicators_7c0731f0.html.
- Edith T. Penrose. *The Theory of the Growth of the Firm*. Basil Blackwell, Oxford, 1959.
- Brian T. Pentland and Martha S. Feldman. Organizational routines as a unit of analysis. *Industrial and Corporate Change*, 14(5):793–815, 2005.

- Brian T. Pentland, Martha S. Feldman, Markus C. Becker, and Peng Liu. Dynamics of organizational routines: A generative model. *Journal of Management Studies*, 49(8):1484–1508, 2012.
- Nils Reimers and Iryna Gurevych. Sentence-BERT: Sentence Embeddings using Siamese BERT-Networks. In *Proceedings of the 2019 Conference on Empirical Methods in Natural Language Processing and the 9th International Joint Conference on Natural Language Processing (EMNLP-IJCNLP)*, pages 3982–3992, Hong Kong, China, 2019. Association for Computational Linguistics.
- Jeanine Romano, Jeffrey D. Kromrey, Jesse Coraggio, and Jeff Skowronek. Appropriate Statistics for Ordinal Level Data: Should We Really Be Using t-test and Cohen’s d for Evaluating Group Differences on the NSSE and Other Surveys? In *Annual meeting of the Florida Association of Institutional Research*, 2006.
- Kaitao Song, Xu Tan, Tao Qin, Jianfeng Lu, and Tie-Yan Liu. MPNet: Masked and Permuted Pre-training for Language Understanding. In *Advances in Neural Information Processing Systems 33 (NeurIPS)*, pages 16857–16867, 2020.
- Michael Webb. The Impact of Artificial Intelligence on the Labor Market. Technical report, SSRN Working Paper, 2020. SSRN 3482150.
- Shitao Xiao, Zheng Liu, Peitian Zhang, Niklas Muennighoff, Defu Lian, and Jian-Yun Nie. C-Pack: Packed Resources For General Chinese Embeddings. In *Proceedings of the 47th International ACM SIGIR Conference on Research and Development in Information Retrieval (SIGIR ’24)*. ACM, 2024. DOI 10.1145/3626772.3657878. Working-paper antecedent: arXiv:2309.07597 (2023). The BGE family (BAAI/bge-large-en-v1.5) is released as part of this package.

A $K = 5$ Robustness Cut

The headline $K = 7$ partition (§3.4) was selected on dendrogram inspection of natural breakpoints. As a robustness backup, we report the raw Ward output at $K = 5$ (the next informative cut below the $K = 7$ headline). The $K = 5$ partition produces five macros:

- $K=5$ **Macro-1** (9 micro-clusters: C5, C6, C7, C8, C10, C15, C24, C26, C28; 2,706 actions, 17.1% of total). Top TF-IDF terms *using, appropriate, secure, don, inspect*. Cog% = 31.9, dominant stage Manipulation_Execution (35%). This macro merges the eventual $K = 7$ M1 (Locating & Provisioning) and M2 (Tool-Mediated Physical) into a single physical block.
- $K=5$ **Macro-2** (singleton C9, the eventual M3 “Iterative Repetition” meta-action layer; 112 actions, 0.7%).
- $K=5$ **Macro-3** (constituting most of the eventual M4 Diagnostic Analysis).
- $K=5$ **Macro-4** (merging the eventual M6 Person-Centred Service and M7 Planning & Design into a single cognitive block).

- $K=5$ **Macro-5** (eventual M5, Verification & Stakeholder Reporting, splits off from the cognitive block at $K = 5$ but not yet from M6/M7).

The physical block ($K=5$ Macro-1) collapses the eventual M1/M2 distinction, and the cognitive block ($K=5$ Macro-4) collapses the eventual M6/M7 distinction. The bipolar shape is therefore visible at $K = 5$ in coarser form: the same physical block sits at the low pole and the same cognitive block sits at the high pole. The $K = 7$ refinement separates M1 from M2 and M6 from M7, exposing the cleaner bipolar contrast we report in the main text. Detailed micro-cluster listings, TF-IDF tables, and stage distributions for the $K = 5$ partition are available in the supplementary file `macro_K5_raw.md`.

B Resolution Sweep Detail ($K = 7, 8, 10, 12, 15$)

Table 9 reports the resolution sweep summary referenced in §4.3. The polar gap widens monotonically with K ; the middle-pair non-significance rate falls. The M2/M7 micro-cluster identities migrate to other macros at $K \geq 10$; the bipolar shape itself persists at every K .

Table 9: Resolution sweep summary. “Polar gap” is the difference between the high-pole and low-pole macro means at each K . “Middle non-sig” is the share of middle-macro pairs that are not Bonferroni-significant.

K	Low pole	High pole	Polar gap	KW H	Middle non-sig
7	M2 (0.055)	M7 (0.502)	0.447	164.6	15/15 = 100%
8	M2 (0.055)	M8 (0.502)	0.447	214.3	13/21 = 61.9%
10	M3 (0.038)	M10 (0.502)	0.464	220.2	20/28 = 71.4%
12	M7 (0.031)	M8 (0.604)	0.573	406.8	22/45 = 48.9%
15	M8 (0.031)	M9 (0.604)	0.573	497.2	44/78 = 56.4%

C TOST Equivalence Test Detail

Equivalence margins were pre-registered: $\delta_d = 0.2 \times \sigma_{\text{pool}} = 0.060$ on the OAI $[0, 1]$ scale (Cohen’s $d = 0.2$ on the pooled middle-six SD $\sigma_{\text{pool}} = 0.2997$), and $\delta_{\text{abs}} = \pm 0.05$. The M2-vs-M7 sanity check returns $p_{\text{TOST}} = 1.000$ under both margins (non-equivalent as required). On the 15 middle pairs, the single pair reaching equivalence at the primary margin is M4 vs Noise ($p_{\text{TOST}} = 0.020$, mean difference 0.017). At the robustness margin (± 0.05 absolute) zero pairs are equivalent. Detail per pair (mean OAI diff and p_{TOST} at both margins) is reproduced in the supplementary file `tost_equivalence.md`.

D Intelligence-Type Robustness: MPNet Cross-Check

The Paper 2 main text reports intelligence-type results under BGE encoding (§4.8). The MPNet labels (the encoder also used for clustering in §3.2) reproduce the qualitative pattern, supporting the encoder-pair robustness claim. Under MPNet labels: overall class distribution Linguistic 52.6%, Multimodal Perception 18.6%, Embodied 17.3%, Human-Bound 11.4% (versus BGE 49.8%/20.5%/16.4%/13.3%). Cohen’s κ for inter-encoder agreement across the 15,817 actions

is 0.666 (substantial agreement; per-class one-vs-rest κ values: Linguistic 0.660, Multimodal Perception 0.683, Embodied 0.738, Human-Bound 0.561).

The MPNet-labelled DWA-level OAI test gives Kruskal-Wallis $H = 509.7$, $p = 3.78 \times 10^{-110}$ across the four intelligence types (versus BGE’s $H = 527.6$, $p = 4.87 \times 10^{-114}$); the LLM-class mean OAI is 0.424 under MPNet versus 0.427 under BGE; the LLM/other-three ratio is $3.49\times$ under MPNet versus $3.37\times$ under BGE. The pairwise Bonferroni-corrected Mann-Whitney pattern matches: the three Linguistic-vs-other pairs are significant under both encoders, with the Embodied-vs-Linguistic contrast at $p_{\text{Bonf}} = 1.8 \times 10^{-66}$ (MPNet) and 1.8×10^{-77} (BGE).

The remaining three middle pairs (Embodied vs Human-Bound, Embodied vs Multimodal Perception, Human-Bound vs Multimodal Perception) reach Bonferroni significance under BGE labels at $p_{\text{Bonf}} \in [7.4 \times 10^{-15}, 2.0 \times 10^{-4}]$ but fail to reject under MPNet labels at $p_{\text{Bonf}} \in [0.05, 1.00]$. This is the second piece of evidence (alongside the human audit, Appendix E) that BGE labels carry better-resolved class boundaries in the borderline cases where the two encoders disagree.

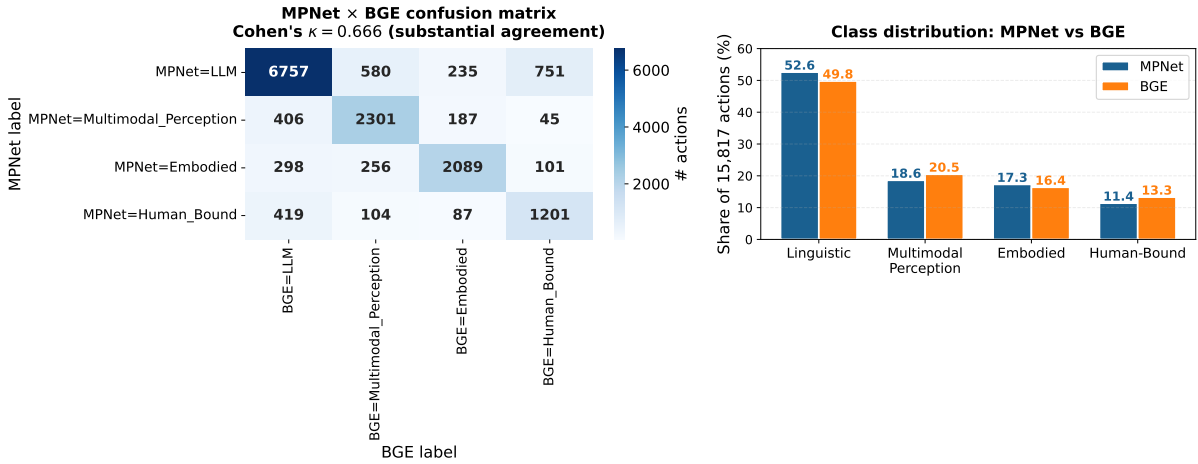


Figure 12: MPNet versus BGE intelligence-type labelling. Left: per-class share under each encoder (Linguistic dominates both, but the smaller classes shift slightly). Right: agreement matrix; the diagonal mass is 78.1% of the 15,817 actions and overall Cohen’s $\kappa = 0.666$ (substantial agreement). The encoder pair check provides a population-level robustness signal independent of the 150-row human audit.

E Human-Audit Detail (Intelligence-Type Validation)

A stratified 150-row sample was drawn from the 15,817 actions, balanced by MPNet label class (~ 37 – 38 actions per class) and further stratified by MPNet/BGE encoder agreement (120 agreement rows + 30 disagreement rows). The author manually labelled each row against the four-class operational definitions, applying a hybrid decision rule: on the 120 encoder-agreement rows, the consensus was accepted by default with three deliberate reversals where the consensus was judged incorrect; on the 30 encoder-disagreement rows, each was adjudicated against the operational definitions independently. Five `human_notes` were written, marking the three consensus reversals plus two disagreement rows where neither encoder selected the correct class.

The audit metrics are summarised in Table 10. BGE matches the human ground truth at $\kappa = 0.893$ (92.0% accuracy); MPNet matches at $\kappa = 0.769$ (82.7%). The 9.3-point accuracy gap concentrates entirely on the 30 disagreement rows: on the 120 encoder-agreement rows, both encoders match the human at 97.5% (only the three deliberate reversals are misses); on the 30 disagreement rows, BGE matches the human at 70% versus MPNet’s 23%. The encoders are essentially equivalent on consensus cases; BGE is markedly better on borderline cases.

Table 10: Human audit metrics (150 rows). Per-class precision / recall / F1 are computed against the human label.

Class	vs MPNet		vs BGE	
	Precision	Recall	Precision	Recall
Linguistic	0.816	0.738	0.886	0.929
Multimodal Perception	0.763	0.906	0.909	0.938
Embodied	0.865	0.889	0.970	0.889
Human-Bound	0.865	0.800	0.925	0.925
Overall accuracy	82.7%		92.0%	
Cohen’s κ	0.769		0.893	

The top human \rightarrow MPNet disagreement modes are Human-Bound mistakenly labelled Linguistic ($n = 5$; e.g., contract signature with legal accountability mis-read as text production); Linguistic mistakenly labelled Multimodal Perception ($n = 5$; e.g., “review the operational manual” mis-read as inspection); and Embodied mistakenly labelled Multimodal Perception ($n = 3$; e.g., “operate the excavator” mis-read as observation). The top human \rightarrow BGE disagreement modes are all at $n \leq 2$ per pair with no systematic concentration, indicating BGE’s residual errors are distributed rather than systematic. Figure 13 visualises both confusion matrices side by side.

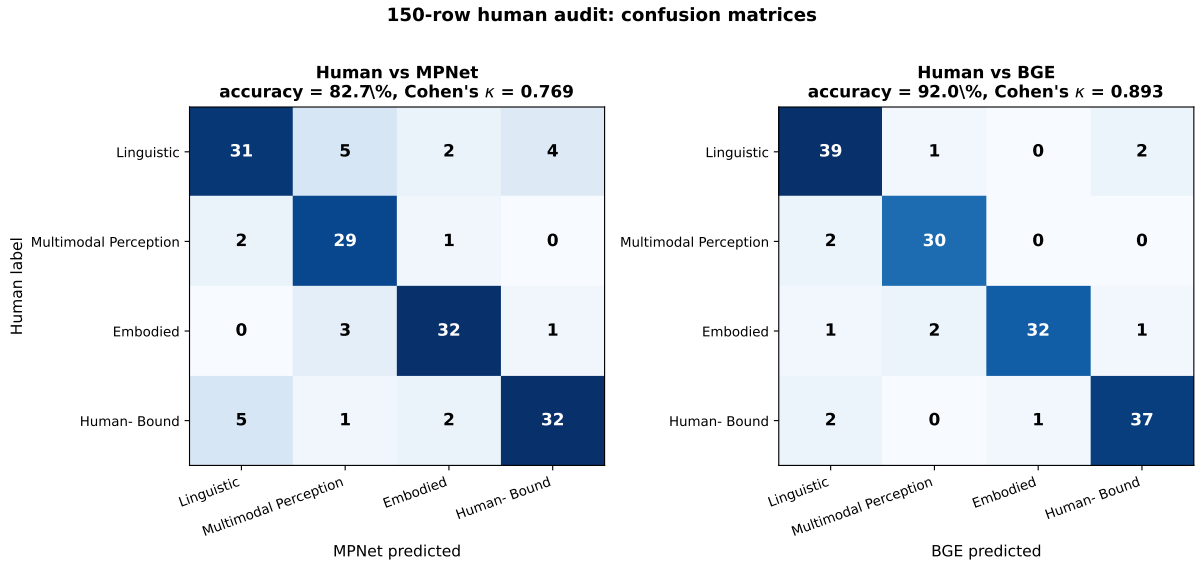


Figure 13: Confusion matrices on the 150-row human audit. Left: human label vs MPNet prediction ($\kappa = 0.769$, accuracy 82.7%); the off-diagonal mass concentrates in the Human-Bound/Linguistic, Linguistic/Multimodal Perception, and Embodied/Multimodal Perception cells. Right: human label vs BGE prediction ($\kappa = 0.893$, accuracy 92.0%); off-diagonal mass is small and uniformly distributed.

F External-Indicator Alignment Detail

Coverage and matching diagnostics for the three external indicators projected onto our 1,961-DWA frame:

Eloundou GPT-4 task labels. Input file `automation_gpt4_human_labels.tsv`; 19,265 rows of (O*NET-SOC, Task ID, gpt4 tier $\in \{T_0 \dots T_4\}$). Tier-to-value mapping is the linear $\{0, 0.25, 0.50, 0.75, 1.0\}$. Tasks joined to DWAs via O*NET 30.2 Tasks to DWAs crosswalk (23,850 rows; 18,796 unique tasks; 2,083 unique DWAs). DWA score is the equal-weight mean of constituent task scores. Coverage: 1,958 of 1,961 DWAs (99.85%).

AIOE. Input file `AIOE_DataAppendix.xlsx`; one value per SOC-2018 six-digit occupation. O*NET-SOC codes mapped to parent SOC-2018 by stripping the two-digit decimal suffix. AIOE value replicated across all SOC \times DWA pairs sharing that SOC; DWA score is the equal-weight mean. Coverage: 1,914 of 1,961 DWAs (97.6%).

Frey-Osborne. Input file `frey_osborne_working_paper.pdf` (Oxford Martin School, 1.3 MB), with the 702-row appendix parsed programmatically (pages 62–78). Validation against the compilation embedded in [Eloundou et al. \(2024\)](#) `autoScores.csv` `freyOsborne` column: Spearman $\rho = 1.000$ across 653 matched SOC codes (Pearson $r = 1.000$; mean $|\Delta| < 0.001$; max $|\Delta| < 0.001$). FO probability mapped to DWAs via SOC \rightarrow OnetSOC \rightarrow DWA equal-weight aggregation. Coverage in the 9-group macro-level era-inversion analysis: 2,019 DWAs (with slight SOC \rightarrow DWA fan-out from the OnetSOC-to-SOC strip).

The DWA-level pairwise Spearman matrix across the four indicators is reproduced in supplementary file `convergence_report.md`; the OAI \leftrightarrow Eloundou correlation is the strongest ($\rho = 0.635$), followed by Eloundou \leftrightarrow AIOE ($\rho = 0.628$). FO correlates negatively with all three LLM-era indicators (OAI $\rho = -0.116$; Eloundou $\rho = -0.221$; AIOE $\rho = -0.567$), consistent with the polarity-inversion finding reported in §5.2.